

# Compositional Controls on the Distribution of Brine in Europa's Ice Shell

N. S. Wolfenbarger<sup>1</sup>, M. G. Fox-Powell<sup>2</sup>, J. J. Buffo<sup>3</sup>, K. M. Soderlund<sup>1</sup>, D. D. Blankenship<sup>1</sup>

<sup>1</sup>Institute for Geophysics, John A. and Katherine G. Jackson School of Geosciences, University of Texas  
at Austin, Austin, Texas, USA

<sup>2</sup>AstrobiologyOU, The Open University, Walton Hall, Milton Keynes, UK

<sup>3</sup>Dartmouth College, Hanover, New Hampshire, USA

## Key Points:

- The brine volume fraction of impure water ice can be represented as a simple polynomial function of temperature and bulk ice salinity.
- For the same temperature and bulk salinity, the brine volume fraction in a Cl-dominated ice shell is higher than a SO<sub>4</sub>-dominated ice shell.
- The magnitude of the percolation threshold governs the minimum fraction of salt entrained in ice formed through freezing of an ocean.

---

Corresponding author: Natalie S. Wolfenbarger, [nwolfenb@utexas.edu](mailto:nwolfenb@utexas.edu)

## Abstract

The composition of impurities in ice controls the stability of liquid water and thus the distribution of potential aqueous habitats. We present a framework for modeling the brine volume fraction in impure water ice as a simple polynomial function of temperature and bulk ice salinity, inspired by models originally developed for sea ice. We applied this framework to examine the distribution of brine within the thermally conductive layer of Europa's ice shell, considering binary (NaCl and  $\text{MgSO}_4$ ) and analog (Cl-dominated and  $\text{SO}_4$ -dominated) endmember impurity compositions. We found that the vertical extent of brine in a conductive ice layer, expressed as a fraction of the total layer thickness, is more sensitive to composition for the binary endmember impurity compositions than for the analog endmember impurity compositions. Although the vertical extent of brine is equal for the analog endmember impurity compositions, the brine volume fraction is consistently higher for the Cl-dominated ice shell than the  $\text{SO}_4$ -dominated ice shell. Pressure, governed by the ice thickness, was found to have only a minor effect on the vertical extent of brine within an ice shell, relative to temperature and bulk salinity. The minimum stable bulk ice shell salinity formed through freezing of an ocean was found to be insensitive to composition and ultimately governed by the magnitude of the assumed percolation threshold.

## Plain Language Summary

When ice forms from salt water, salt is excluded from the ice causing the remaining liquid water to become more saline, forming brine. We developed a method to build models that estimate how much brine, solid salt, and ice exist at a certain temperature for a certain amount of salt. Because water is a necessary ingredient for life, places where brine exists in ice represent potential habitats. We applied our method to the ice shell of Jupiter's moon Europa, assuming it formed from an ocean made up of different types of dissolved salts and mixtures of salts. We found that the depth where brine is stable in an ice shell is more sensitive to the type of salt when two ions are present than when four ions are present. When the salt is made mostly of chloride, a larger volume of brine exists than when the salt is made up mostly of sulfate. The thickness of the ice shell did not affect the percentage of the ice layer where brine existed as much as temperature or the amount of salt did. The type of salt in the ocean did not affect how much salt was retained in the ice.

## 1 Introduction

The presence of liquid water has long guided the search for life beyond Earth (Des Marais et al., 2008). Once thought to be confined to the “Goldilocks zone”, vast oceans have been inferred to exist beneath the thick ice shells of moons in the outer solar system (Hand et al., 2020). Although these sub-ice oceans represent the most compelling potential habitats in the outer solar system (Shematovich, 2018), they are covered by ice shells that can range from kilometers to hundreds of kilometers thick (Soderlund et al., 2020). Impurities within the ice shell, such as salts, acids, or organic compounds, could allow for liquid water to remain stable at temperatures well below that predicted by the pressure-melting curve of pure water (Marion et al., 2003, 2005; Ruiz et al., 2007). Salt impurities in particular support the formation of intra-ice shell brine pockets, which could represent potential habitats that might be more accessible than the sub-ice ocean (Kargel et al., 2000; Marion et al., 2003).

Impurities are incorporated into Europa’s ice shell either by accretion of oceanic material at the ice-ocean interface (endogenic) (Buffo et al., 2018; Zolotov & Shock, 2001; Wolfenbarger et al., in press), or the introduction of material at the surface through impactors or implantation by Io’s plasma torus (exogenic) (Carlson et al., 2009; Brown & Hand, 2013; Ligier et al., 2016; Hendrix et al., 2011). Whereas exogenic impurities are sulfur-dominated, the composition of endogenic impurities is less well constrained. Putative magnesium sulfate salts detected at the surface were originally thought to be derived from the ocean due to their correlation with young features (McCord et al., 1998). However, higher spectral resolution Earth-based measurements using the W. M. Keck Observatory challenged this interpretation, finding that although the magnesium may be endogenic, the sulfates were likely exogenic (Brown & Hand, 2013). Subsequent measurements using the Hubble Space Telescope revealed signatures of sodium chloride correlated to resurfacing features, suggesting an oceanic origin (Trumbo et al., 2019). In this work we focus on endogenic impurities and leave exogenic impurities to future work. Ultimately, the composition of the ice shell resulting from entrainment of ocean material is governed by the composition of the sub-ice ocean and processes operating within the ice shell that may promote fractionation, such as flushing by drainage of meltwater generated from tidal or shear heating (Wolfenbarger et al., in press). As such, although we have constraints on the composition of surface impurities, there is still ambiguity to whether Europa’s ocean is dominated by magnesium sulfate or sodium chloride salts.

Here we present a framework for modeling the brine volume fraction in ice, inspired by models developed for terrestrial sea ice (Cox & Weeks, 1983). Whereas previous methods have used freezing experiments to obtain properties of intra-ice brine as a function of temperature (Assur, 1960; Cox & Weeks, 1983), we employ the open source aqueous geochemistry program FREZCHEM (Marion & Kargel, 2007). For temperatures below the eutectic, brine is no longer stable; however, residual salts can serve as an indicator of relict water systems and thus as a signature of former potential habitats. As such we also consider the salt volume fraction and propose a model for its calculation in conjunction with brine volume fraction. A major motivation for the development of the proposed framework is to facilitate the incorporation of more complex chemical species in geophysical investigations of ocean worlds. Representing the chemical evolution of brine as it freezes using polynomial functions translates the complex output of geochemistry software to a more broadly accessible form, facilitating multi-disciplinary research that is key to advancing the field of astrobiology.

We apply our model to Europa’s ice shell, although the approach can be applied to impure water ice of any composition. Our approach is validated by comparing against existing models for the brine volume fraction of sea ice. The distribution of thermodynamically stable brine for a thermally conductive ice layer of arbitrary thickness is evaluated. A linear temperature is assumed to represent both the case of a conductive lid and conductive ice shell. Initially we consider two binary endmember compositions: NaCl and  $\text{MgSO}_4$  (Section 3.1) before we increase the geochemical complexity and consider multi-component systems with compositions more representative of natural waters that incorporate endmember compositions for Europa’s ocean (Section 3.2). These more complex compositions are referred to as analog endmember compositions and represent a chloride-dominated and a sulfate-dominated European ocean. The influence of ice shell thickness (i.e., pressure) on the vertical extent of brine for the assumed linear temperature profile is examined for the analog endmember compositions (Section 3.3). The role of composition in governing bulk ice shell salinity is explored (Section 3.4), motivated by previous studies which argued that permeability, governed by brine volume fraction, may represent a critical parameter (Buffo et al., 2020, 2021; Wolfenbarger et al., in press).

Although the scope of this work is focused on Europa’s ice shell, estimating the distribution of brine in an ice shell represents an important step in studying the holistic habitability of Europa, as well as other ocean worlds. The brine volume fraction governs a

number of bulk ice shell thermophysical properties, such as density, thermal conductivity, specific heat capacity, and viscosity. These thermophysical properties in turn govern processes of surface-ice-ocean exchange, thought to be important for Europa’s habitability. Because the brine volume fraction also governs bulk dielectric properties, building models for the distribution of brine in Europa’s ice shell represents critical context for interpretation of ice-penetrating radar data collected by the upcoming JUICE and Europa Clipper missions (D. D. Blankenship et al., 2009; D. Blankenship et al., 2018; Bruzzone et al., 2013).

## 2 Methods

Impure ice is a multiphase, multicomponent system made up of solid ice, solid salts, liquid water, dissolved salts (i.e., ions), and trapped gases. The volume of brine stable in ice is governed by the bulk salinity of the ice, the temperature, and the composition of the salts. Representing the brine volume fraction as a function of these parameters requires knowledge of the phase behaviour (i.e., the concentration or mass of ionic species, brine, ice, and precipitates). Methods developed to model the brine volume fraction in sea ice, which represents the most ubiquitous and well-studied form of saline ice on Earth, serve as a foundation to develop models for saline ice on other worlds.

### 2.1 Equations for Modeling the Brine Volume Fraction of Sea Ice

An equation for the brine volume fraction of sea ice as a function of temperature,  $T$ , can be obtained from the relationships presented in Cox and Weeks (1983) (see SI 1.1) and is given by

$$\frac{V_b}{V}(T) = \left(1 - \frac{V_a}{V}(T)\right) \frac{\rho_i(T)S}{F_1(T) - \rho_i(T)SF_2(T)}, \quad (1)$$

where  $\frac{V_b}{V}$  is the brine volume fraction,  $\frac{V_a}{V}$  is the gas volume fraction,  $\rho_i$  is the density of pure water ice in units of g/cm<sup>3</sup>, and  $S$  is the bulk salinity of the ice in units of ppt (i.e., weight percent expressed in g/kg solution). Note that for this work, we neglect the presence of trapped gases and assume  $\frac{V_a}{V} = 0$ .  $F_1$  and  $F_2$  are functions representing the properties of terrestrial seawater between the pure ice pressure melting temperature,  $T_m$ , and the eutectic temperature,  $T_{eut}$ . These phase behavior functions are defined as

$$F_1(T) = \rho_b(T)S_b(T)(1 + k(T)) \quad (2)$$

where  $\rho_b$  is the brine density in units of g/cm<sup>3</sup>,  $S_b$  is brine salinity in units of ppt, and  $k$  is the ratio of the mass of solid salts (excluding bound water molecules) to the mass of dissolved salts in the brine, and

$$F_2(T) = (1 + C(T))\frac{\rho_b(T)}{\rho_i(T)} - \frac{C(T)\rho_b(T)}{\rho_{ss}(T)} - 1 \quad (3)$$

where  $\rho_{ss}$  is the density of solid salts (i.e., precipitates) in units of g/cm<sup>3</sup> and  $C$  is the ratio of mass of solid salts to the mass of brine. In the original model of Cox and Weeks (1983), they assume a constant salt density of  $\rho_{ss} = 1.5$  g/cm<sup>3</sup>; however, here we use  $\rho_{ss}$  to represent the total salt density as a function of temperature (see SI 1.2). Note that the temperature dependence of  $\rho_{ss}$  represented here reflects the changing composition of salts, which are used to calculate the total density. We assume the density of an individual salt mineral is temperature invariant. The salt volume fraction can be expressed in terms of the brine volume fraction (where brine is stable) using an additional phase behavior function, which we define as  $F_3$ . The expression for the salt volume fraction is given by

$$\frac{V_{ss}}{V}(T) = F_3(T)\frac{V_b}{V}(T) \quad (4)$$

where  $\frac{V_{ss}}{V}$  is the salt volume fraction,  $\frac{V_b}{V}$  is the brine volume fraction, and

$$F_3(T) = C(T)\frac{\rho_b(T)}{\rho_{ss}(T)}. \quad (5)$$

Note that in the work of Cox and Weeks (1983) they do not explicitly define a phase behavior function for the salt volume fraction as we do here, likely because the salt volume fraction is often negligible in sea ice applications.

These equations allow the brine volume fraction and salt volume fraction of impure water ice to be represented as a function of bulk ice salinity and temperature for the temperature range where brine is stable in the ice (i.e., from the pure ice pressure melting temperature to the eutectic temperature). Accordingly, the values of the phase behavior functions at the pure ice pressure melting temperature are  $F_1(T = T_m) = 0$ ,  $F_2(T =$

$T_m) = \frac{\rho_w(T=T_m)}{\rho_i(T=T_m)} - 1$ , and  $F_3(T = T_m) = 0$ , where  $\rho_w$  represents the density of pure water. Although these phase behavior functions are defined up to the pure ice pressure melting temperature, ice will not be stable at the pure ice pressure melting temperature for a bulk ice salinity greater than 0 ppt. The presence of salts will cause the freezing temperature to be lower than the pure ice pressure melting temperature (i.e., freezing point depression occurs when impurities are present).

A feature of this model is that the predicted brine volume fraction exceeds unity (non-physical) as the temperature increases beyond the freezing temperature for a specified bulk ice salinity. For example, this model predicts the brine volume fraction of 10 ppt sea ice will exceed unity at  $-0.054$  °C which corresponds to the freezing temperature for 10 ppt terrestrial seawater. At temperatures which far exceed the freezing temperature, the model will transition from predicting brine volume fractions above unity to negative brine volume fractions (also non-physical). These non-physical brine volume fractions can be redefined as unity since they indicate conditions (temperature and bulk salinity) where ice is not thermodynamically stable and the solution is entirely liquid.

The phase behavior functions,  $F_1$  and  $F_2$ , for terrestrial seawater were originally derived using the phase equilibrium table of Assur (1960), based off the experimental data of Nelson and Thompson (1954) and Ringer (1906). These experiments studied the phase behavior as a function of temperature for a solution composition representative of standard terrestrial seawater. Although data were collected down to  $-54$  °C, the phase behavior functions were only defined down to  $-30$  °C, likely because this represented the temperature range of interest for terrestrial seawater. Later work using the open source aqueous geochemical modeling tool, FREZCHEM, demonstrated that the so-called Ringer-Nelson-Thompson (RNT) freezing pathway constructed by Assur (1960) may not be representative of the thermodynamically stable pathway for the freezing of terrestrial seawater (Marion et al., 1999). Instead, equilibrium freezing of terrestrial seawater appears to follow the experimental data of Gitterman (1937) which were unfortunately excluded from the work of Assur (1960) because the data were not available to him. More recent studies of the freezing of artificial sea ice brines have been consistent with the Gitterman pathway (Geilfus et al., 2013; Butler & Kennedy, 2015).

The major difference between these two pathways is the eutectic temperature, which is a consequence of the early precipitation of gypsum ( $\text{CaSO}_4 \cdot 2\text{H}_2\text{O}$ ) along the Gitter-

man pathway (Marion et al., 1999). As a result of this, the Gitterman pathway reaches the eutectic at  $-36.2\text{ }^{\circ}\text{C}$  with the precipitation of magnesium chloride dodecahydrate ( $\text{MgCl}_2 \cdot 12\text{H}_2\text{O}$ ), whereas the RNT pathway reaches the eutectic at  $-53.8\text{ }^{\circ}\text{C}$  with the precipitation of antartcite ( $\text{CaCl}_2 \cdot 6\text{H}_2\text{O}$ ). Practically, this implies brine in sea ice is not thermodynamically stable below temperatures of  $-36.2^{\circ}\text{C}$ . A detailed study of these two freezing pathways can be found in Marion et al. (1999). Although FREZCHEM has been leveraged to study the freezing of terrestrial seawater for a number of works since its inception (Vancoppenolle et al., 2019; Geilfus et al., 2013; Butler et al., 2016), the phase diagram of Assur (1960) still represents the basis for modeling the brine volume fraction of sea ice to this day (Petrich & Eicken, 2017). For application to an ice shell, the difference in eutectic temperatures resulting from the freezing pathways and/or composition could translate to differences on the order of kilometers in predictions of vertical brine extent, highlighting the importance of composition in both geophysical and astrobiological investigations.

## 2.2 A Framework for Modeling the Distribution of Brine in Saline Ice

Although the equations in Section 2.1 were originally derived for application to sea ice, the approach is fundamentally agnostic to the solution composition, which can be represented by the phase behavior functions,  $F_1$ ,  $F_2$ , and  $F_3$ . Furthermore, the advent of aqueous geochemistry software, such as FREZCHEM and PHREEQC, provides access to virtual laboratories where freezing experiments can be conducted for saline water anywhere on Earth and across the solar system. Only a single freezing simulation is needed to obtain the phase behavior functions for a given composition, analogous to the single dataset which represents the basis for the phase behavior functions for terrestrial seawater. For this work we employ FREZCHEM version 15.1 for all freezing simulations with the exception of terrestrial seawater, where we use version 13.3. For terrestrial seawater, version 15.1 fails to converge where meridianiite should begin to precipitate and thus is unable to simulate freezing down to the eutectic temperature.

All FREZCHEM simulations were conducted assuming an initial temperature of  $0\text{ }^{\circ}\text{C}$  (273.15 K) and a temperature decrement of 0.1 K. An initial temperature of  $0\text{ }^{\circ}\text{C}$  was chosen to ensure that the onset of ice formation would be captured. We define the eutectic temperature as the temperature associated with the final convergent temperature step, as opposed to the temperature where FREZCHEM fails to converge. The pa-

rameters  $k$ ,  $C$ ,  $\rho_b$ , and  $S_b$  as a function of temperature can be derived from the FREZCHEM output file, which contains the solution composition and mineral phases at temperatures ranging from the initial temperature, specified in the input file, to the eutectic temperature, where the model no longer converges. The densities of solid salts are not directly output; however, molar volumes for each salt mineral are incorporated into the software and documented in the literature (Marion et al., 2005, 2012). These molar volumes are assumed to be independent of temperature and pressure. To ensure the phase behavior functions are properly defined across the temperature domain ranging from the pure ice pressure melting temperature to the eutectic temperature, only a subset of the temperature steps within that domain are extracted from the FREZCHEM output file. Temperature steps above the freezing point are excluded since they represent solution properties at a fixed salinity. Figure 1 presents a flowchart illustrating the framework for modeling the volume fraction of ice, brine, and solid salts leveraging the output of aqueous geochemistry software.

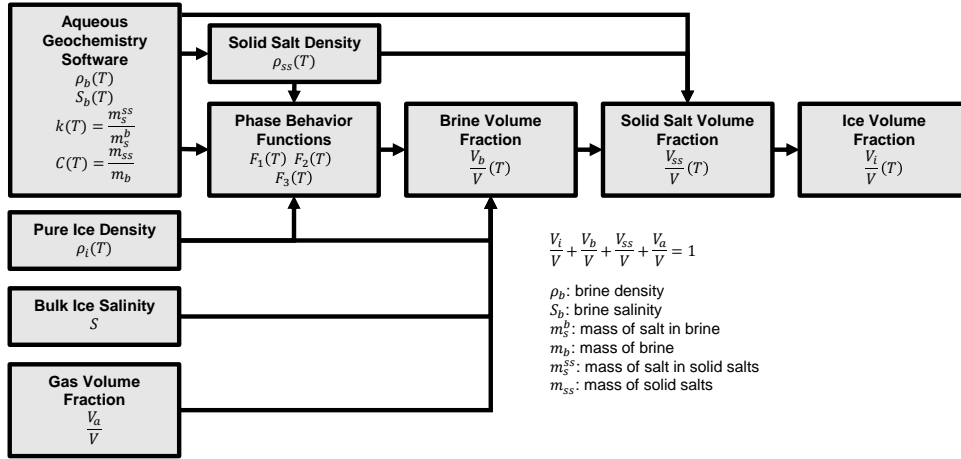


**Figure 1.** Flowchart describing our framework for modeling the volume fraction of brine and salt in saline ice.

A major advantage of this framework is that bulk ice salinity is decoupled from the composition of impurities, allowing a single model for impure ice of a specified composition to be applied over a range of possible bulk ice salinity. However, to obtain the phase behavior functions for a specified composition, an initial solution concentration must be assumed. In the case of sea ice, recall that the original phase behavior functions were derived from experimental data from the freezing of 35 ppt terrestrial seawater. To ex-

amine the influence of the initial salinity on the phase behavior functions for a specified solution composition, we conducted a sensitivity study. Figure 2 illustrates the phase behavior functions derived from FREZCHEM simulations of terrestrial seawater (Millero et al., 2008) over a temperature range from 0 °C to  $-36.2$  °C. The seawater salinity (i.e., the brine salinity at the pure ice pressure melting temperature,  $S_b(T = T_m)$ ) specified in the input file is varied to study the sensitivity of the phase behavior functions to the initial solution concentration. Note that the phase behavior functions shown here are truncated at the freezing temperature instead of extending to the pure ice pressure melting temperature, to show where the curves are overlapping. Although  $F_2(T)$  and  $F_3(T)$  are not influenced by the seawater salinity,  $F_1(T)$  starts to exhibit appreciable differences when the salinity exceeds 100 ppt.

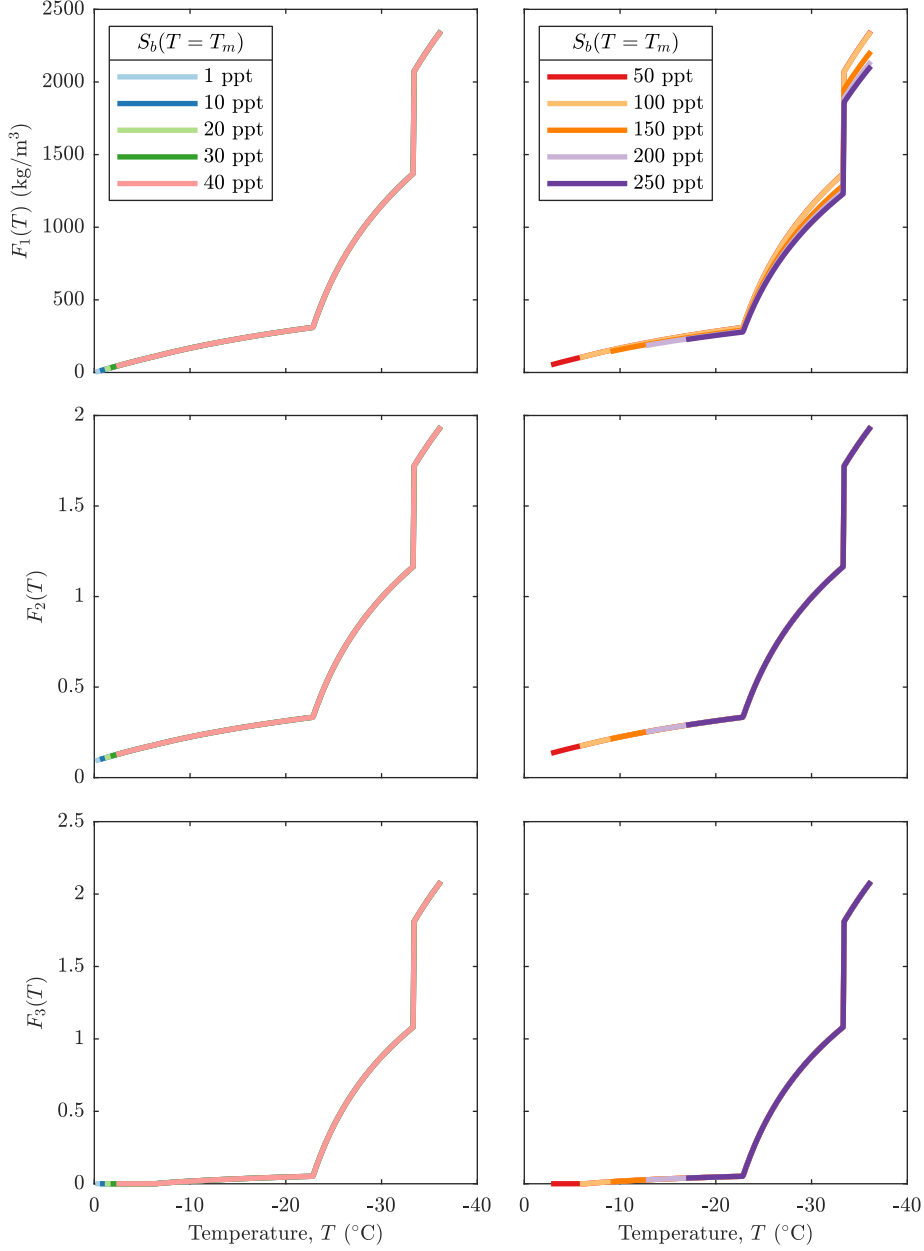


**Figure 2.** Phase behavior functions derived from FREZCHEM simulations of terrestrial seawater, assuming a range of salinities  $S_b(T = T_m)$ .

The source of the discrepancy in  $F_1(T)$  above 100 ppt can be attributed to the  $k$  term in Eq. (2). A higher  $k$  at a given temperature will cause a relative decrease in  $F_1(T)$ . Because  $k$  represents a quantification of salt precipitation normalized by the amount of dissolved salts in the brine, it is affected by changes in the salt precipitation sequence.

Table 1 presents the temperature at which each salt begins to precipitate as terrestrial seawater freezes for the cases shown in Fig. 2. Below 100 ppt, the salt precipitation sequence is not influenced by the initial seawater salinity. Above 100 ppt, seawater is supersaturated with respect to certain salt minerals, specifically ikaite ( $\text{CaCO}_3 \cdot 6\text{H}_2\text{O}$ ) for an initial seawater salinity  $\geq 100$  ppt, gypsum ( $\text{CaSO}_4 \cdot 2\text{H}_2\text{O}$ ) for an initial seawater salinity  $\geq 150$  ppt, and mirabilite ( $\text{Na}_2\text{SO}_4 \cdot 10\text{H}_2\text{O}$ ) for an initial seawater salinity  $\geq 150$  ppt. Supersaturation causes the salt to precipitate at the first temperature step in the FREZCHEM simulation ( $T = 0^\circ\text{C}$ ). The supersaturation of ikaite which occurs for an initial seawater salinity  $\geq 100$  ppt does not appear to noticeably affect  $F_1(T)$ , because the mass of ikaite which precipitates is negligible relative to the mass of dissolved salts in the brine. However for an initial seawater salinity  $\geq 150$  ppt, the combined mass of ikaite and gypsum precipitating at the first temperature step is no longer negligible relative to the mass of dissolved salts in the brine. Additionally, because the ion activities are higher at the first temperature step due to a higher initial concentration, a greater total mass of solid salts precipitate at the first temperature step, increasing  $k$  and thus decreasing  $F_1(T)$  at every temperature step.

| $S_b(T = T_m)$ (ppt)                                | 1                                       | 10    | 20    | 30    | 40    | 50    | 100        | 150        | 200        | 250        |
|---|---|-------|-------|-------|-------|-------|------------|------------|------------|------------|
|   | Temperature, $T$ ( $^{\circ}\text{C}$ ) |       |       |       |       |       |            |            |            |            |
| <i>Ikaite</i>                                       |   |       |       |       |       |       |            |            |            |            |
| $\text{CaCO}_3 \cdot 6\text{H}_2\text{O}$           | -4.9                                    | -4.9  | -4.9  | -4.9  | -4.9  | -4.9  | $\geq 0.0$ | $\geq 0.0$ | $\geq 0.0$ | $\geq 0.0$ |
| <i>Gypsum</i>                                       |   |       |       |       |       |       |            |            |            |            |
| $\text{CaSO}_4 \cdot 2\text{H}_2\text{O}$           | -6.2                                    | -6.2  | -6.2  | -6.2  | -6.2  | -6.2  | -6.2       | $\geq 0.0$ | $\geq 0.0$ | $\geq 0.0$ |
| <i>Mirabilite</i>                                   |   |       |       |       |       |       |            |            |            |            |
| $\text{Na}_2\text{SO}_4 \cdot 10\text{H}_2\text{O}$ | -6.4                                    | -6.4  | -6.4  | -6.4  | -6.4  | -6.4  | -6.4       | -3.4       | -1.0       | $\geq 0.0$ |
| <i>Hydrohalite</i>                                  |   |       |       |       |       |       |            |            |            |            |
| $\text{NaCl} \cdot 2\text{H}_2\text{O}$             | -22.9                                   | -22.9 | -22.9 | -22.9 | -22.9 | -22.9 | -22.9      | -22.9      | -22.9      | -22.9      |
| $\text{NaBr}$                                       | -22.9                                   | -22.9 | -22.9 | -22.9 | -22.9 | -22.9 | -22.9      | -22.9      | -22.9      | -22.9      |
| <i>Meridianiite</i>                                 |   |       |       |       |       |       |            |            |            |            |
| $\text{MgSO}_4 \cdot 11\text{H}_2\text{O}$          | -33.3                                   | -33.3 | -33.3 | -33.3 | -33.3 | -33.3 | -33.3      | -33.3      | -33.3      | -33.3      |
| <i>Sylvite</i>                                      |   |       |       |       |       |       |            |            |            |            |
| $\text{KCl}$  | -33.4                                   | -33.4 | -33.4 | -33.4 | -33.4 | -33.4 | -33.4      | -33.4      | -33.4      | -33.4      |
| $\text{MgCl}_2 \cdot 12\text{H}_2\text{O}^a$        | -                                       | -     | -     | -     | -     | -     | -          | -          | -          | -          |

**Table 1.** The temperature at which a specified salt starts precipitating for terrestrial seawater of salinity,  $S_b(T = T_m)$  at a pressure of 1 atm, predicted by FREZCHEM v13.3. Note that for a seawater salinity greater than 100 ppt certain salts begin precipitating at higher temperatures, influencing the phase behavior functions shown in Fig. 2. <sup>a</sup>Our version of FREZCHEM v13.3 fails to display text that  $\text{MgCl}_2 \cdot 12\text{H}_2\text{O}$  is precipitating at/beyond the eutectic, possibly due to a compiler issue; however this is known from previous works (Marion et al., 1999; Vancoppenolle et al., 2019). We also note that this text appears to be absent in the FREZCHEM v13.3 output files of some other authors (see Vancoppenolle et al. (2019)).

There are two important takeaways of the sensitivity study shown in Fig. 2 and Table 1: (i) the phase behavior functions are independent of the initial solution salinity, so long as the initial solution is sufficiently dilute (i.e., the solution is not supersaturated with respect to any salt) and (ii) the phase behavior functions are defined over a larger temperature domain for a lower initial solution salinity. Because terrestrial seawater has a salinity of approximately 35 ppt, the phase behavior functions were origi-

nally only defined for temperatures up to the freezing point of terrestrial seawater ( $T_f \approx -2^\circ\text{C}$ ). The domain of the phase behaviour functions was eventually extended up to the pure ice pressure melting temperature of  $0^\circ\text{C}$  (Leppäranta & Manninen, 1988), to represent more dilute solutions with relative compositions equivalent to terrestrial seawater (e.g., sea ice formed from the brackish waters of the Baltic Sea). This extension of the phase behavior functions to the pressure-melting temperature essentially amounts to interpolating the phase behavior functions between the freezing point to the pure ice pressure melting temperature. These extended phase behavior functions are analogous to the liquidus in simple binary systems, where brine density and brine salinity decrease to pure water as the temperature increases to the pure ice pressure melting point and the brine density and brine salinity increase to the eutectic as the temperature decreases.

### 2.3 Validation through Comparison to Sea Ice

We validate our brine volume fraction model through comparison to the existing sea ice brine fraction model (Petrich & Eicken, 2017), originally obtained by Cox and Weeks (1983) and augmented by Leppäranta and Manninen (1988). We use FREZCHEM v13.3 to derive the phase behavior functions for terrestrial seawater, represented by the composition of Millero et al. (2008) in Marion et al. (2009). Figure 3 presents a comparison of the brine salinity, brine density, and phase behavior functions between the two models. The circles in the brine salinity curve are extracted directly from the phase equilibrium table of Assur (1960). The solid black curves in each plot depict the output of FREZCHEM. Note that because the FREZCHEM simulations are run for a specified impurity concentration (i.e., initial salinity), the phase behavior functions can only be defined from FREZCHEM output up to the solution freezing temperature, where ice begins to form (e.g.,  $T_f \approx -2^\circ\text{C}$  for 35 ppt terrestrial seawater). To extend the domain of the phase behavior functions to the pure ice pressure melting temperature, we define an additional data point at the pure ice pressure melting temperature, corresponding to the value of the phase behavior functions for a brine salinity of zero and a brine density equivalent to that of pure water (see Section 2.1). The black dashed curves depict the existing model for sea ice. The vertical dotted lines depict the temperatures at which salts begin to precipitate as the solution freezes. The thin red curves represent the phase behavior functions we derived by fitting piecewise polynomial functions of temperature to the FREZCHEM output (Table S1). The kinks in the phase behavior func-

tions correspond to major precipitation events that occur along the freezing pathway, mainly the formation of hydrohalite ( $\text{NaCl} \cdot 2\text{H}_2\text{O}$ ) at  $-22.9^\circ\text{C}$  and meridianiite ( $\text{MgSO}_4 \cdot 11\text{H}_2\text{O}$ ) at  $-33.3^\circ\text{C}$ . The brine density model used in the existing approach assumes a linear dependence of brine density on brine salinity, originally proposed by Zubov (1945), whereas our model extracts the brine density and brine salinity directly from the FREZCHEM output file.

Our model derived using FREZCHEM, presented in Table S1, agrees well with the existing model for temperatures above  $-22.9^\circ\text{C}$ , where hydrohalite begins to precipitate. For temperatures below  $-22.9^\circ\text{C}$ , our phase behavior functions exceed those derived by Cox and Weeks (1983). This deviation is in part due to the underprediction of brine density in the existing model relative to that estimated by FREZCHEM. An additional expected source of discrepancy is the freezing pathway. The FREZCHEM output is more representative of the Gitterman pathway, whereas the dataset of Assur (1960) is more representative of the RNT pathway. Our model extends the temperature domain where the brine volume fraction can be calculated for sea ice to below  $-30^\circ\text{C}$ . Although for Earth applications this temperature range may only be relevant under extreme conditions, defining the phase behavior functions over the entire temperature domain where brine is stable is critically relevant for application to the ice shells of ocean worlds.

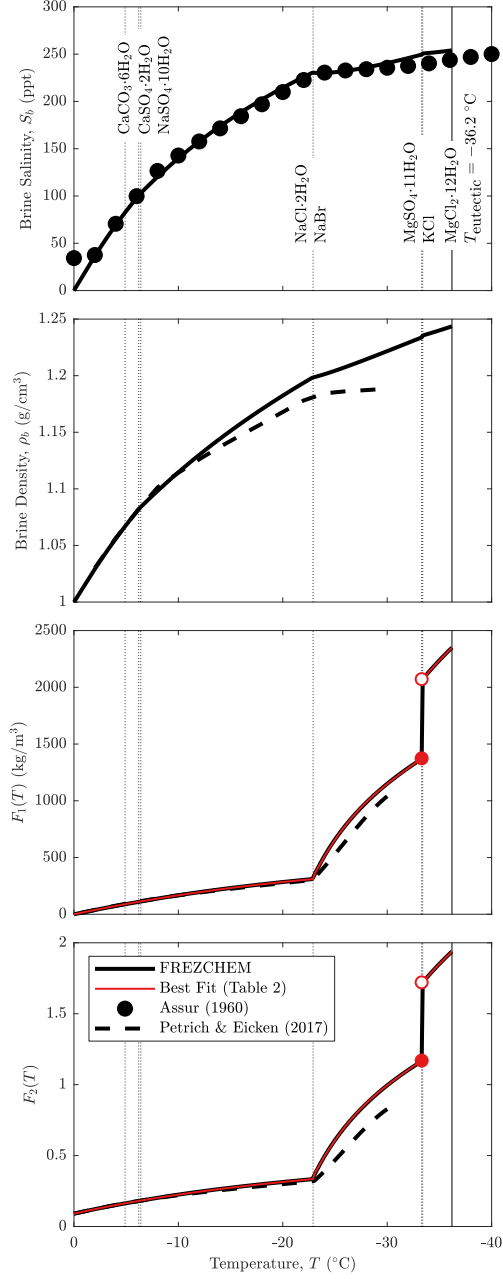


**Figure 3.** Validation of our framework through comparison of the phase behavior functions ( $F_1(T)$  and  $F_2(T)$ ), brine density ( $\rho_b$ ), and brine salinity ( $S_b$ ). The vertical dotted lines illustrate the temperature where a mineral (specified in the top panel) first begins to precipitate. The black solid curves represent values from FREZCHEM output, the black dashed curves represent the existing model of Petrich and Eicken (2017), and the thin red curves represent the model derived in this work (Table S1).

Figure 4 presents a comparison of the brine volume fraction estimate for sea ice using our phase behavior functions in Table S1 and the phase behavior functions in the existing model of Petrich and Eicken (2017).  $S = 5$  ppt is chosen because it represents a typical bulk salinity for sea ice and because of its significance to the “golden rule of fives” (Golden et al., 1998), where at a bulk salinity of 5 ppt, the brine volume fraction is 5% at  $-5$  °C. Instead of assuming a linear temperature dependence for the pure ice density term in Eq. (1), as is typically assumed (Petrich & Eicken, 2017), we use the equation of state for ice Ih released by the International Association for the Properties of Water and Steam (IAPWS) in IAPWS R10-06(2009), originally published by Feistel and Wagner (2006). We similarly use the equation of state for water released by the IAPWS in IAPWS SR7-09(2009), originally published by Feistel (2008), to obtain the density of water term needed to define  $F_2(T = T_m)$  in Eq. (3). Similarly to Fig. 3, we use dotted lines to represent temperatures where salts begin to form as the solution freezes. Our estimated brine volume fractions are in good agreement with those predicted by the existing model for temperatures above  $-22.9$  °C. The model of Cox and Weeks (1983) predicts a slightly increased brine volume fraction at a given temperature relative to our model.

Importantly, both models are consistent with the “golden rule of fives”, depicted as a yellow star in Fig. 4. The brine volume fraction of 0.05, often referred to as a critical porosity, is an important parameter in sea ice desalination models because it represents an apparent percolation threshold (Petrich et al., 2011; Turner et al., 2013; Buffo et al., 2018). Below a brine volume fraction of 0.05, convection-driven desalination no longer occurs due to a significant reduction in permeability (Golden et al., 1998, 2007; Pringle et al., 2009). This critical porosity applies to congelation sea ice, which is characterized by columnar ice crystals that grow parallel to the temperature gradient (Golden et al., 1998; Wolfenbarger et al., in press). The agreement between our model and the existing model for sea ice validates our approach to use aqueous geochemistry software to derive phase behavior functions to model the brine volume fraction of ice formed through the freezing of oceans on other worlds.

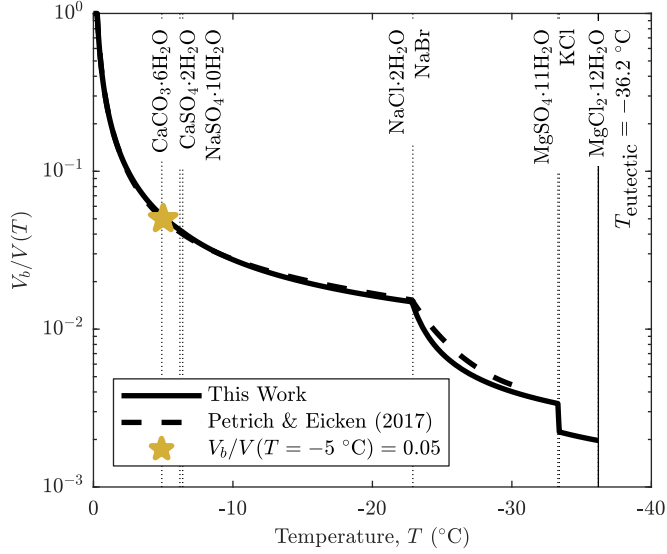


**Figure 4.** Brine volume fraction as a function of temperature for sea ice of bulk salinity  $S = 5$  ppt. The vertical dotted lines illustrate the temperature where each mineral starts to precipitate. The solid curves represent the values derived in this work and the dashed lines represent the existing model. The yellow star illustrates the “golden rule of fives”.

## 2.4 Estimating the Salt Volume Fraction below the Eutectic Temperature

Below the eutectic temperature (i.e., where brine is not thermodynamically stable), the salt volume fraction can be estimated using the expected mass fraction of solid salts at the eutectic temperature. Although FREZCHEM specifies which minerals are precipitating at/beyond the eutectic, it does not calculate the amount of each mineral precipitating. For a binary system (e.g., NaCl) estimating the mass fraction of solid salts at/beyond the eutectic is trivial since ions are contributing to only one non-ice mineral. For example, a 1 molal solution of NaCl, corresponding to a solution salinity of 55 ppt, will yield 1 mole of NaCl·2H<sub>2</sub>O, which translates to a solid salt mass fraction of 89 ppt. Because the mass of NaCl·2H<sub>2</sub>O is higher than NaCl, the weight percent is higher. To obtain an estimate of the total mass of solid salts at/beyond the eutectic for more complex solutions, we must account for all salts which are precipitating (see SI 1.3). We define a scale factor,  $k^*$ , which represents the ratio of the total mass of solid salts at the eutectic to the initial mass of dissolved salts in solution prior to any ice formation. This scale factor is necessary because although the total mass of ionic impurities does not change

as the solution freezes (i.e., mass is conserved), the salt minerals that precipitate can be hydrated (i.e., include bound water molecules) so the total mass of solid salts at the eutectic can exceed the initial mass of dissolved salts.  $k^*$  thus accounts for the hydration of all minerals that precipitate as the solution freezes, including those which form at/beyond the eutectic. To obtain an estimate of the salt volume fraction below the eutectic temperature, an estimate of the salt density is also needed. We calculate a total salt density, incorporating the estimate of solid salts formed at the eutectic, from the FREZCHEM output file. We can express the salt volume fraction in terms of these variables as

$$T_{eut} = \frac{Sk^*}{Sk^* + (1000 - Sk^*) \frac{\rho_{ss}(T=T_{eut})}{\rho_i(T)}} \quad (6)$$

where  $S$  is the bulk ice salinity in units of ppt and  $\rho_{ss}(T = T_{eut})$  is the density of solid salts (i.e., precipitates) in units of g/cm<sup>3</sup> at the eutectic temperature.

## 2.5 Accounting for the Influence of Pressure

One limitation of our approach is that the pressure is assumed to be fixed (i.e., the pressure dependence of phase behavior is not modeled). This is not an appropriate assumption for modeling the stability of brine where ice shells exceed a certain thickness, and the influence of overburden pressure is no longer negligible. One atmosphere of pressure, the pressure assumed in the brine volume fraction estimated for sea ice in Fig. 4, is the pressure equivalent to  $\sim 100$  meters of ice at Europa, which could represent  $< 1\%$  of the total ice shell thickness. Earlier work has studied the influence of pressure on brine chemistry, specifically with application to Europa (Marion et al., 2005). Here we discuss how the phase behavior functions are affected by pressure.

To robustly account for the influence of pressure for any solution, the phase behavior functions must instead be represented as a surface instead of a curve (i.e., a function of both temperature and pressure instead of solely temperature). The surfaces are generated from multiple FREZCHEM simulations for a given composition, where the pressure specified in the input file is varied over the pressure range of interest. Figure 5 is a graphical representation of the phase behavior surfaces for terrestrial seawater. These surfaces were generated using seven FREZCHEM simulations, assuming pressures of 1, 10, 100, 200, 300, 400, and 500 bar. Note that for a pressure of 1 atm, the surfaces would collapse to the curves in Fig. 3.

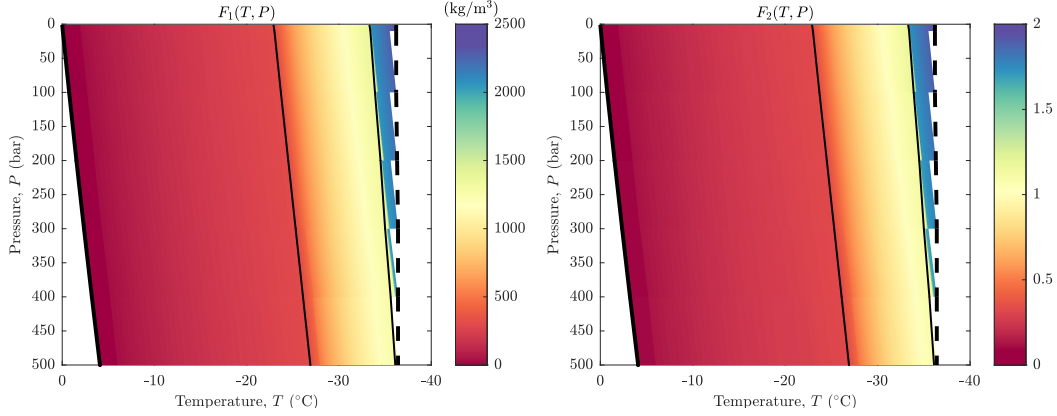


**Figure 5.** The surfaces defining the phase behavior functions for terrestrial seawater. The solid black curve represents the pure ice pressure-melting temperature and the dashed black curve represents the eutectic temperature. The thin black curves are where meridianiite and hydrohalite first begin to form, with hydrohalite forming at a higher temperature than meridianiite.

## 2.6 Temperature Profile

To model the distribution of brine within Europa’s ice shell for an assumed composition, a temperature profile must also be assumed. The thermal state of Europa’s ice shell is unknown; however, studies have shown that the ice shell is either convective, likely in the stagnant lid regime, or fully conductive (Mitri & Showman, 2005; McKinnon, 1999; Hussmann & Spohn, 2004). We note that early studies of heat transfer in Europa’s ice shell constrained the maximum thickness for a conductive ice shell to be approximately 30 km (Ojakangas & Stevenson, 1989; Squyres et al., 1983), whereas later works incorporating the influence of convection estimate a maximum thickness  $\sim 10$  km for either a conductive lid or conductive ice shell (Kalousová et al., 2017; Tobie et al., 2003; Howell, 2021). For this work we assume a conductive temperature profile to represent both the case of a fully conductive ice shell and a conductive lid overlying a convective layer (Fig. 6).

Previous work has shown that the temperature of the convective layer is likely above the eutectic temperature for many salts, suggesting that brine is likely stable throughout the convective layer (Kalousová et al., 2017). Other works have demonstrated that even in the absence of salts, partial melting driven by tidal heating could be pervasive throughout a convective layer (Tobie et al., 2003; Vilella et al., 2020). The tendency for

convection to increase the temperature of a large fraction of the ice shell, as well as to modify the ice rheology through deformation-induced recrystallization (Barr & McKinnon, 2007), could conspire to enhance brine drainage relative to an overall cooler conductive lid that might retain the columnar crystal structure characteristic of a directionally thickening ice layer (Wolfenbarger et al., in press). If brine drainage is efficient throughout a convective layer, the layer will progressively desalinate and trend towards pure ice. As such we assume the same basal temperature for both the conductive lid and the conductive ice shell. To model a scenario representative of the maximum vertical brine extent, we thus assume (i) a surface temperature of  $-173.15\text{ }^{\circ}\text{C}$  (100 K), approximately equal to the mean annual equatorial surface temperature at Europa, (ii) a basal temperature of  $0\text{ }^{\circ}\text{C}$  (273.15 K), the maximum pressure-melting temperature across a range of possible conductive ice layer thicknesses, and (iii) a linear temperature profile. Assuming a basal temperature of  $0\text{ }^{\circ}\text{C}$  implies the brine volume fraction will be unity for some fraction of the ice layer if the pressure exceeds 1 atm or the bulk salinity is greater than 0 ppt. In other words, part of our domain can include the uppermost layer of the ocean. For quantities that are expressed in terms of fraction of the total ice layer thickness, we account for the fact that the base of the ice layer is at a temperature governed by the pressure, bulk ice salinity, and (in the conductive ice shell case) ocean salinity.

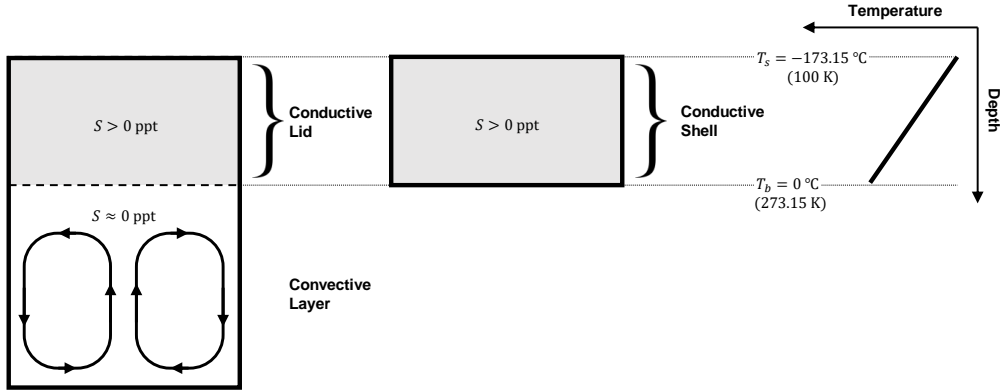


**Figure 6.** Temperature profile for the conductive layer of Europa's ice shell. The assumed profile applies to both the case of a conductive lid overlying a convective layer and a conductive ice shell. The surface temperature,  $T_s$ , basal temperature,  $T_b$ , and linear profile represent a specific hypothesis that maximizes the vertical brine extent within the ice shell.

### 3 Results

We model the brine volume fraction as a function of temperature and salinity for four cases: 1) NaCl, 2) MgSO<sub>4</sub>, 3) a hypothetical Cl-dominated ocean, and 4) a hypothetical SO<sub>4</sub>-dominated ocean. Cases 1 and 2 represent the simple binary endmember compositions for Europa's ocean; whereas, cases 3 and 4 represent more realistic endmember compositions inspired by existing geochemical models, consistent with materials observed at Europa's surface. The NaCl-dominated ocean is a simplified version of terrestrial seawater (Millero et al., 2008), and the MgSO<sub>4</sub>-dominated ocean is a simplified version of the Europa K1a model of Zolotov and Shock (2001). We consider a range of bulk ice salinities, up to the eutectic salinity, assuming a fixed pressure of 1 atm. Recall that we assume a linear temperature profile such that the surface temperature is  $-173.15^{\circ}\text{C}$  (100 K) and the basal temperature is  $0^{\circ}\text{C}$  (273.15 K). Assuming the existence of a percolation threshold, constraints on bulk ice salinity are obtained both for sea ice and for the four cases of ice shell composition. We then analyze the sensitivity of brine volume fraction estimates to total conductive ice layer thickness (i.e., pressure), assuming a fixed bulk salinity of 1 ppt.

#### 3.1 Binary Endmember Ice Shell Compositions

Figure 7 presents the brine and salt volume fraction of binary endmember compositions for Europa's ice shell: NaCl (left) and MgSO<sub>4</sub> (right). The maximum allowable bulk ice salinity is defined by the eutectic salinity (232 ppt for NaCl and 172 ppt for MgSO<sub>4</sub>). We impose this constraint since the bulk ice salinity cannot exceed the eutectic salinity via cryoconcentration for binary systems. The phase behavior functions used to calculate the brine volume fraction are provided in Table S2. For estimating the salt volume fraction below the eutectic, we find  $k^* = 1.6165$  and  $\rho_{ss}(T = T_{eut}) = 1.630 \text{ g/cm}^3$  for NaCl and  $k^* = 2.6463$  and  $\rho_{ss}(T = T_{eut}) = 1.446 \text{ g/cm}^3$  for MgSO<sub>4</sub>. Note that because these are binary solutions, the solid salt density at the eutectic simply corresponds to the density of hydrohalite and meridianite for NaCl and MgSO<sub>4</sub>, respectively. The thick dashed line illustrates the eutectic temperature and the thick solid curve represents the liquidus (i.e., the temperature above which the brine volume fraction is unity for a given bulk ice salinity). The thin dotted line indicates the temperature where the brine volume fraction first exceeds 0.05 for a given bulk ice salinity. Below the eutectic temperature the ice shell is composed of solid salt (hydrohalite for NaCl and meridianite

for  $\text{MgSO}_4$ ) and ice, whereas above the eutectic temperature the ice shell is composed of brine and ice.

The vertical extent of brine is greater for  $\text{NaCl}$  than  $\text{MgSO}_4$  due to its lower eutectic temperature. For both cases, the maximum brine volume fraction at the eutectic increases as the bulk ice salinity increases. Although the eutectic salinity of  $\text{NaCl}$  is higher than  $\text{MgSO}_4$ , because the density of hydrohalite is greater than meridianiite ( $1.63 \text{ g/cm}^3$  vs.  $1.44 \text{ g/cm}^3$ ) the maximum salt volume fraction is greater for  $\text{MgSO}_4$ . Although we are able to estimate the brine volume fraction for ice shells of a bulk salinity up to the eutectic salinity, the bulk salinity is limited by the efficiency of salt entrainment into the ice shell (Wolfenbarger et al., in press). More locally, cryoconcentration of perched lakes or sills could generate regions of enhanced bulk salinity (Chivers et al., 2021). Rapid freezing of ocean water, such as through rifts in the ice shell, could also locally increase the bulk ice salinity (Buffo et al., 2020; Wolfenbarger et al., in press).

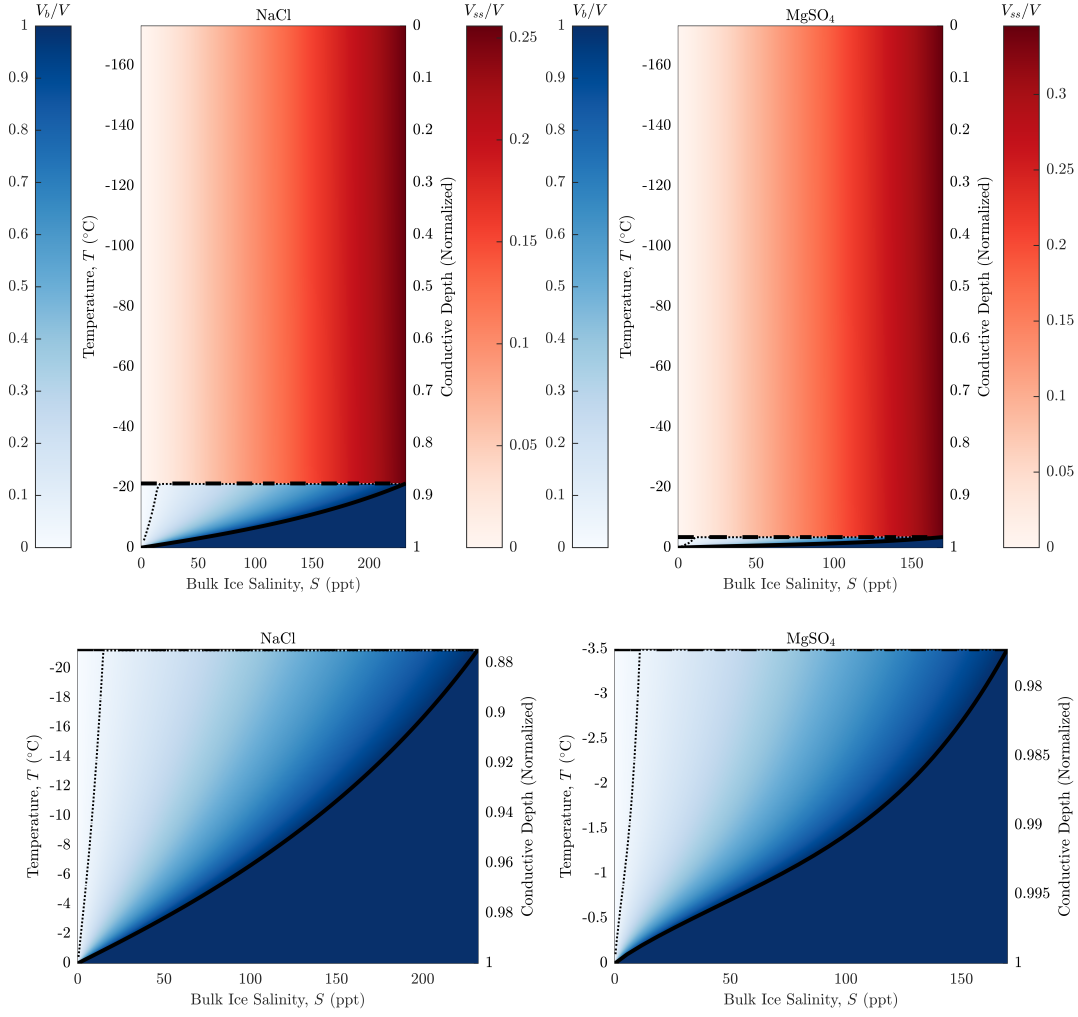


**Figure 7.** Brine volume fraction for Europa’s ice shell assuming binary endmember compositions for the ocean and a fixed pressure of 1 atm. The vertical axis corresponds to the temperature at a given depth within the ice shell. The thick dashed line illustrates the eutectic temperature and the thick solid curve represents the brine salinity as a function of temperature (i.e., the liquidus). The thin dotted curve corresponds to a brine volume fraction of 0.05.

### 3.2 Analog Endmember Ocean Compositions

Although the cases considered in Fig. 7 are representative of the endmember compositions hypothesized for Europa, because the eutectic temperatures differ by almost an order of magnitude, the influence of composition on the distribution of brine is significant. The sensitivity to composition in the binary case likely does not represent the reality at Europa, where multiple salt minerals and ionic species have been detected at

the surface and in the atmosphere. Where multiple ionic species are present in a brine, precipitation events alter the brine composition such that it becomes progressively enriched in more soluble species (which precipitate at lower temperatures/ higher concentrations) as the solution freezes. For example, we expect a sulfate enriched brine to become progressively more enriched in chlorides since sulfates salts tend to precipitate at higher temperatures than chloride salts. We thus consider compositions that are more representative of natural waters, simplified to four major ionic species ( $\text{Na}^+$ ,  $\text{Cl}^-$ ,  $\text{Mg}^{2+}$ ,  $\text{SO}_4^{2-}$ ). Of the many possible charge-balanced permutations of these species, two compositions were selected because they (i) share the same eutectic temperature ( $-32.2^\circ\text{C}$ ) and (ii) they are analogous to existing or modeled oceans. We note that the other charge-balanced permutations of these species resulted eutectic temperatures of either  $-32.2^\circ\text{C}$  or  $-35.3^\circ\text{C}$ . Our Cl-dominated case is analogous to the terrestrial seawater composition of Millero et al. (2008), whereas our  $\text{SO}_4$ -dominated case is analogous to the hypothesized European ocean composition of Zolotov and Shock (2001).

The compositions of each ocean are provided in Table 2. For this work we assume the ice shell composition reflects that of the ocean, leaving fractionation to a future work. The concentrations in Table 2 were obtained by approximating the relative concentrations of Zolotov and Shock (2001) and Millero et al. (2008), maintaining charge balance, and fixing the total concentration to 0.1 molal (i.e., ensuring the starting solution is relatively dilute). Table 2 also identifies which salts precipitate as the solutions freeze, as well as the temperature at which they begin precipitating. The differences in the salt precipitation sequence between these two compositions can be attributed to the relative abundances of the ions. In both cases the ion activity product of sodium and sulfate becomes sufficiently high and exceeds the equilibrium constant at relatively high temperatures, triggering mirabilite precipitation. This occurs at a higher temperature in the  $\text{SO}_4$ -dominated case since the limiting ion ( $\text{Na}^+$ ) has a higher relative abundance than the limiting ion in the Cl-dominated case ( $\text{SO}_4^{2-}$ ). The subsequent precipitation of hydrohalite in the Cl-dominated case occurs because mirabilite serves as a sink of an already limited supply of sulfate, preventing the precipitation of meridianiite until later in the sequence when the solution becomes more cryoconcentrated and the activity is sufficiently high to trigger meridianiite precipitation. In the  $\text{SO}_4$ -dominated case, meridianiite precipitates at a much higher temperature since mirabilite precipitation is sodium-limited, resulting in an abundance of free sulfate to trigger the precipitation of merid-

528 ianiite. The formation of hydrohalite in the Cl-dominated case and the formation of merid-  
 529 ianiite in the SO<sub>4</sub>-dominated case represent the two most significant precipitation events,  
 530 from the perspective of relative mass of solid salts forming, and as such coincide to the  
 531 breakpoints in the phase behavior functions (Table S3 and S4).

532 Figure 8 presents the brine volume fraction of the analog endmember compositions  
 533 for Europa’s ice shell: Cl-dominated (left) and SO<sub>4</sub>-dominated (right). The phase be-  
 534 havior functions used to calculate the brine volume and salt volume fraction are provided  
 535 in Table S3 and S4. For estimating the salt volume fraction below the eutectic, we find  
 536  $k^* = 1.8439$  and  $\rho_{ss}(T = T_{eut}) = 1.5827 \text{ g/cm}^3$  for the Cl-dominated case and  $k^* =$   
 537  $2.5175$  and  $\rho_{ss}(T = T_{eut}) = 1.456 \text{ g/cm}^3$  for the SO<sub>4</sub>-dominated case. Unlike in the  
 538 binary cases in Fig. 7, the salt volume fraction is non-zero above the eutectic temper-  
 539 ature and calculated using Eq. (4). Although the solid black curve in Fig. 8 also rep-  
 540 resents the brine salinity as a function of temperature, it is not a true liquidus (defined  
 541 as the temperature above which a solution is entirely liquid) since salt minerals may be  
 542 stable at higher temperatures if the solution salinity is sufficiently high. Recall that this  
 543 is not an issue for binary solutions since salts only precipitate via cryoconcentration at  
 544 the eutectic. As such for temperatures above this “pseudo-liquidus”, the brine volume  
 545 fraction may be non-unity and salt volume fraction may be non-zero. Similarly, although  
 546 we define the upper bound of our salinity domain as the brine salinity at the eutectic  
 547 temperature, this likely does not represent the maximum possible bulk ice salinity since  
 548 solid salts are also present.

549 Like the binary cases in Fig. 7, the thick dashed line illustrates the eutectic tem-  
 550 perature and the thin dotted line indicates the temperature where the brine volume frac-  
 551 tion first exceeds 0.05 for a given bulk ice salinity. The kinks in the brine salinity curves  
 552 indicate where significant salt precipitation events occur and cause the brine salinity to  
 553 decrease (e.g., hydrohalite for the Cl-dominated case and meridianiite for the SO<sub>4</sub>-dominated  
 554 case). Our analog endmember compositions suggest that brine is likely stable for a larger  
 555 vertical extent in the ice shell than predicted by simple binary compositions, regardless  
 556 of which species are dominant. Although these analog endmember compositions share  
 557 the same eutectic temperature, brine is present at a higher volume fraction throughout  
 558 the Cl-dominated ice shell than the SO<sub>4</sub>-dominated ice shell, whereas the opposite is true  
 559 for salt volume fraction. The high brine volume fraction stable for the Cl-dominated ice  
 560 shell is likely due to the late (i.e., at lower temperatures) precipitation of hydrohalite that

occurs even when the activities of  $\text{Na}^+$  and  $\text{Cl}^-$  are high, coupled with the fact that a much larger fraction of water is consumed by precipitation of meridianiite relative to hydrohalite (11 vs. 2 moles of water per mole of hydrate). Additionally, the tendency for sulfates to precipitate early (i.e., at higher temperatures) does not favor the stability of brine for the  $\text{SO}_4$ -dominated ice shell.

| Cl-Dominated  |                           |   | SO <sub>4</sub> -Dominated |                |
|---|---------------------------|---|----------------------------|----------------|
|   | Concentration<br>(mol/kg) | Molar<br>Ratio                                      | Concentration<br>(mol/kg)  | Molar<br>Ratio |
| Na <sup>+</sup>                                     | 0.04390                   | 43.9%   | 0.02308                    | 23.1%          |
| Mg <sup>2+</sup>                                    | 0.00488                   | 4.9%  | 0.03077                    | 30.8%          |
| Cl <sup>-</sup>                                     | 0.04878                   | 48.8%   | 0.00769                    | 7.7%           |
| SO <sub>4</sub> <sup>2-</sup>                       | 0.00244                   | 2.4%  | 0.03846                    | 38.4%          |
| Total   | 0.1                       |   | 0.1                        |                |
| Salts Precipitating                                 |                           |   |                            |                |
| Na <sub>2</sub> SO <sub>4</sub> ·10H <sub>2</sub> O | −6.1 °C                   | Na <sub>2</sub> SO <sub>4</sub> ·10H <sub>2</sub> O | −3.4 °C                    |                |
| NaCl·2H <sub>2</sub> O                              | −22.5 °C                  | MgSO <sub>4</sub> ·11H <sub>2</sub> O               | −5.7 °C                    |                |
| MgSO <sub>4</sub> ·11H <sub>2</sub> O               | −32.3 °C                  | NaCl·2H <sub>2</sub> O                              | −32.3 °C                   |                |

**Table 2.** Analog endmember compositions for Europa’s ocean. The Cl-dominated case represents a simplified version of terrestrial seawater, whereas the SO<sub>4</sub>-dominated case represents a simplified version of the K1a ocean of Zolotov and Shock (2001).

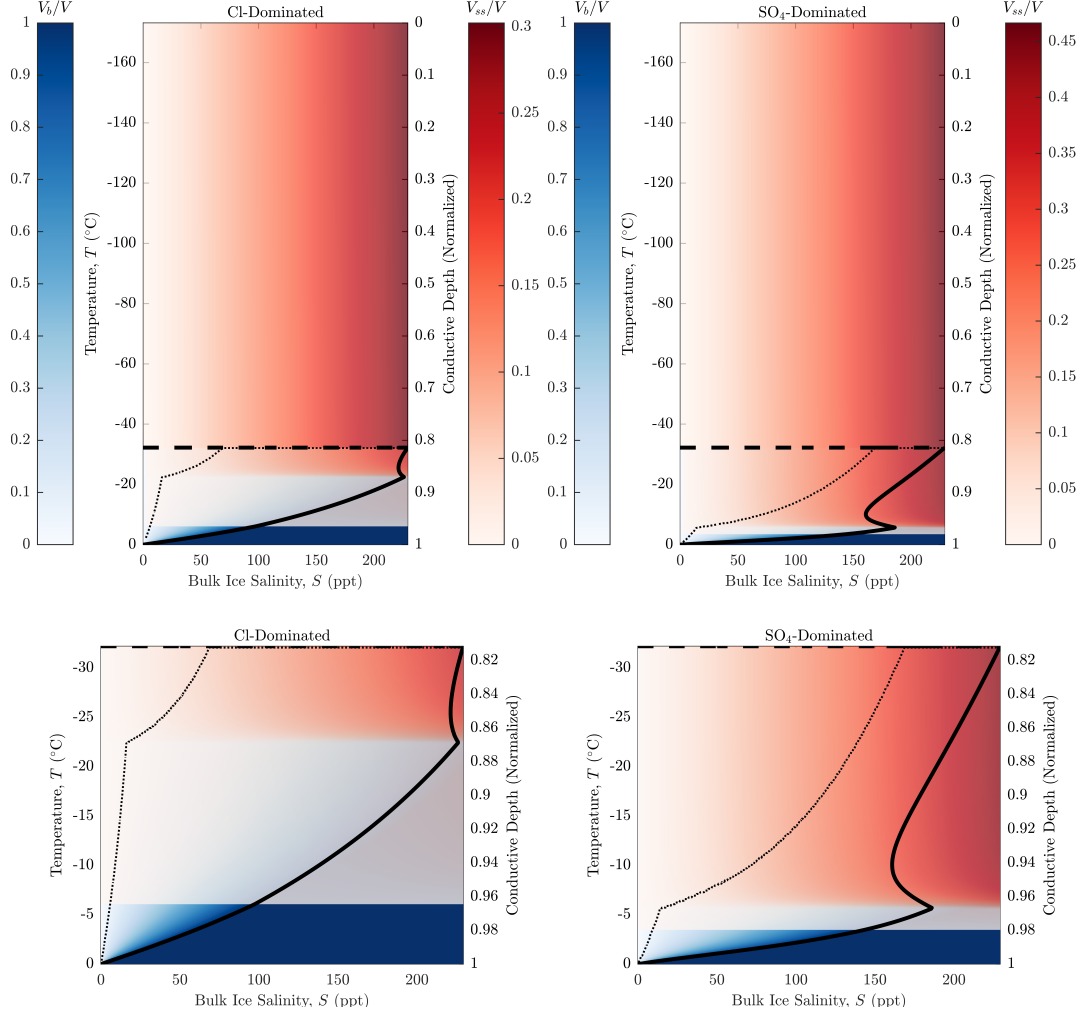


**Figure 8.** Brine volume fraction for a conductive ice layer at Europa assuming analog end-member compositions for the ocean and a fixed pressure of 1 atm. The vertical axis corresponds to the temperature at a given depth within the ice shell. The thick dashed line illustrates the eutectic temperature and the thick solid curve represents the brine salinity as a function of temperature. The thin dotted curve corresponds to a brine volume fraction of 0.05. The red color illustrating salt volume fraction is muted relative to the colorbar due to an imposed transparency which allows both the brine and salt phases to be visible where they are both stable between the eutectic and freezing temperature.

### 3.3 Sensitivity to Pressure

Figures 7 and 8 represent the brine and salt distribution in an ice shell where overburden pressure is neglected and a fixed pressure of 1 atm is assumed throughout. We

now incorporate the effect of ice thickness to examine the sensitivity of the distribution of brine to pressure. The influence of pressure is considered only for the analog endmember compositions and not the binary endmembers since the binary cases are more sensitive to pressure but are likely less realistic for a natural system.

Figure 9a presents the brine volume fraction for a 1 ppt conductive ice layer at Europa assuming analog endmember compositions for the ocean and a range of possible conductive layer thicknesses. 1 ppt represents an order of magnitude estimate for bulk ice salinity formed through freezing of a 10 ppt ocean (Wolfenbarger et al., in press). The pressure at a given depth within the conductive layer is estimated by integrating the temperature-dependent ice density as a function of depth. Note that the conductive layer thickness applies to the entire temperature domain. Recall that we define the base of our domain as 0 °C (273.15 K) and as such (i) ice is not stable at this temperature for certain conductive layer thickness due to the reduction in pressure melting temperature and (ii) if the conductive ice layer overlies an ocean (as opposed to a pure ice convective layer) then the brine volume fraction curves will be truncated such that they equal unity below the ocean freezing temperature, which is governed by the ocean salinity.

Although the brine volume fraction curves shift upwards (lower in temperature) with increasing ice thickness, the general shape of the profile for each composition does not change significantly. This is highlighted in Fig. 9b where the brine volume fraction curves appear to overlap when they are plotted against the relative temperature, defined here as the difference between the absolute temperature (the y-axis in Fig. 9a) and the pure ice pressure melting temperature. Interestingly, because the eutectic temperatures (shown as the thin dashed lines in Fig. 9a) are not as sensitive to pressure as the melting temperature, larger ice thicknesses translate to a lower vertical brine extent, defined as the fraction of the total conductive ice layer thickness. For the range of conductive layer thicknesses considered here, Fig. 9c shows this effect is relatively minor (<1% of the conductive ice layer thickness), and the fraction of the conductive ice layer where brine is stable for the assumed temperature profile is between 18% and 19%.

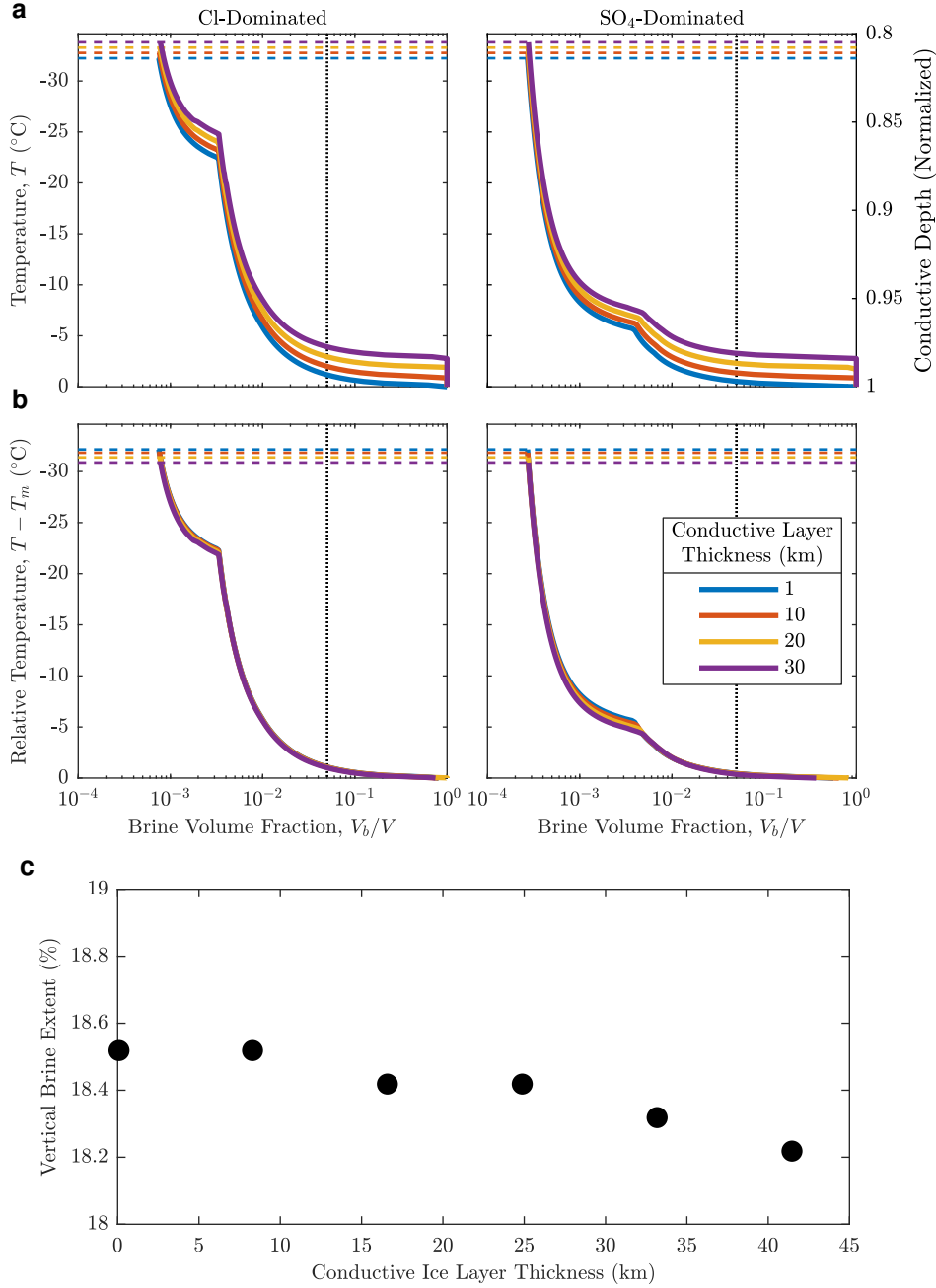


**Figure 9.** Influence of pressure on the distribution of brine in the bottom 20% of the conductive layer for our analog endmember compositions. (a) Brine volume fraction for a 1 ppt conductive ice layer at Europa assuming analog endmember compositions for the ocean and a range of possible ice thicknesses. The thin dashed lines represent the eutectic temperature for a given ice thickness. The top row shows the brine volume fraction for the conductive layer as a function of temperature whereas the bottom row shows the brine volume fraction as a function of relative temperature, defined as the difference between the temperature and the pressure-melting temperature. (b) Fraction of the conductive ice layer where brine is stable as a function of conductive ice layer thickness for both of the analog endmember compositions assumed for Europa's ocean.

### 3.4 Constraints on the “Stable” Bulk Ice Shell Salinity

Previous studies focused on constraining Europa’s ice shell salinity have used inferences based on the assumption of brine pocket migration in an impact crater (Steinbrügge et al., 2020), numerical models developed for sea ice desalination (Buffo et al., 2020), or studied ice formed in environments that could be analogous to Europa’s ice-ocean interface, such as ice accreted beneath terrestrial ice shelves in Antarctica (Wolfenbarger et al., in press). The latter two studies demonstrated that the bulk salinity for an ice shell which forms through freezing of a sub-ice ocean should approach a lower limit referred to as the “asymptotic” bulk salinity in Buffo et al. (2020) and the “stable” salinity in Wolfenbarger et al. (in press).

In the model of Buffo et al. (2020), the asymptotic bulk salinity reflected an imposed cutoff in permeability (i.e., percolation threshold) at a brine volume fraction of 0.05, consistent with the critical porosity for congelation sea ice referenced in Section 2.3. The later work of Buffo et al. (2021) did not directly impose a percolation threshold, but used a permeability-porosity relationship derived for sea ice which exhibits significantly reduced permeability at brine volume fractions less than 0.05. Although some authors argue that the existence of a percolation threshold in sea ice prevents desalination for brine volume fractions below the critical porosity (Golden et al., 1998, 2007), others argue that the desalination mechanism transitions from an efficient convection-dominated process known as gravity drainage to a less efficient diffusion-dominated process (Buffo et al., 2020, 2021).

Wolfenbarger et al. (in press) examined the salinity profiles of low temperature gradient ice cores to obtain constraints on the fraction of salt entrained in ice formed through slow freezing of an ocean. They represented this fraction using an effective equilibrium solute distribution coefficient, defined as the ratio of the stable salinity of ice, derived from the salinity profiles, normalized by the salinity of the underlying ocean ( $k_{eq} = S_{ice}/S_{ocean}$ ). Wolfenbarger et al. (in press) noted that there was a similarity between the value they derived for the effective equilibrium solute distribution coefficient and the critical porosity for congelation sea ice. They interpreted this similarity as evidence supporting that a percolation threshold likely governed the effective equilibrium solute distribution coefficient. Because the critical porosity reflects a volume fraction whereas the solute distribution coefficient represents a mass fraction, these quantities are not directly compa-

629 rable; however, our brine volume fraction model allows us to explore the relationship be-  
 630 tween these quantities while ensuring thermodynamic compatibility.

631 Figure 10a illustrates the dependence of sea ice brine volume fraction on bulk ice  
 632 salinity and temperature. The region in blue signifies temperatures above the freezing  
 633 point for 35 ppt terrestrial seawater. The dashed line represents the percolation thresh-  
 634 old at a brine volume fraction of 0.05. Curves to the right of the dashed line, within the  
 635 gray area, reflect ice that is still highly permeable, and thus presumably in an active state  
 636 of desalination. Curves to the left of the dashed line are effectively impermeable and no  
 637 longer undergoing convection-driven desalination. This plot suggests that the bulk salin-  
 638 ity of newly formed sea ice subject to a percolation threshold of 0.05 cannot fall below  
 639 approximately 2 ppt, since convection-driven desalination cannot occur below this salin-  
 640 ity even at the warmest possible temperature where ice can form (i.e., the freezing tem-  
 641 perature).

642 Because sea ice forms in a high temperature gradient environment, salt entrainment  
 643 is facilitated by the progression of a freezing front which traps brine interstitially and  
 644 prevents continued drainage. As such, the stable bulk salinity of sea ice is typically higher  
 645 than 2 ppt ( $\sim 5$  ppt). The arrows in Fig. 10a represent an illustration of a possible de-  
 646 salination pathway which produces sea ice with a stable bulk salinity of 5 ppt, adapted  
 647 from Petrich and Eicken (2017). A higher temperature gradient freezing pathway would  
 648 fall below the red curve, whereas a lower temperature gradient pathway would appear  
 649 above the red curve.

650 Recognizing that brine drainage will outpace the freezing front at the very low growth  
 651 velocities expected at Europa’s ice-ocean interface (Wolfenbarger et al., in press), we can  
 652 leverage the existence of a percolation threshold to constrain the stable bulk ice shell salin-  
 653 ity. The bulk ice salinity that results in a brine volume fraction equal to the critical poros-  
 654 ity, at the ocean freezing temperature, represents a minimum bound for salt entrainment  
 655 in ice where desalination is subject to a percolation threshold. This condition can be ex-  
 656 pressed mathematically using Eq. (1) to obtain

$$\phi_c = \frac{V_b}{V}(T_f(S_{ocean})) = \frac{\rho_i(T_f(S_{ocean}))S_{ice}}{F_1(T_f(S_{ocean})) - \rho_i(T_f(S_{ocean}))S_{ice}F_2(T_f(S_{ocean}))}, \quad (7)$$

where  $\phi_c$  is the critical porosity (brine volume fraction) that defines the percolation threshold,  $T_f$  is the ocean freezing temperature, governed by the ocean salinity,  $S_{ocean}$ , and  $S_{ice}$  is the stable bulk ice shell salinity. Compatible with previous works, we first assume the percolation threshold occurs at a brine volume fraction of 0.05. As such, we consider the bulk ice salinity that results in a brine volume fraction of 0.05 at the freezing temperature, for a given ocean salinity and composition, to represent the stable bulk salinity of the ice shell.

If we apply this criteria to terrestrial seawater at 35 ppt, we obtain a bulk ice salinity estimate of 1.95 ppt. This corresponds to the bulk salinity curve which intersects both the dotted line and the lower boundary of the blue region in Fig. 11. This is notably the bulk ice salinity obtained using the constitutive equation of Buffo et al. (2018) for the freezing of terrestrial seawater in the “diffusive regime” (i.e., where ice is transitioning to being effectively impermeable), although we note they assume a seawater salinity of 34 ppt. The bulk salinity of 1.95 ppt obtained here is lower than the bulk ice salinity found for the “sub-ice-shelf congelation ice” samples studied by Wolfenbarger et al. (in press), which ranged from 2.2 to 2.35 ppt. To produce a stable bulk ice salinity of 2.35 ppt using this methodology, a critical porosity of 0.062 would be required.

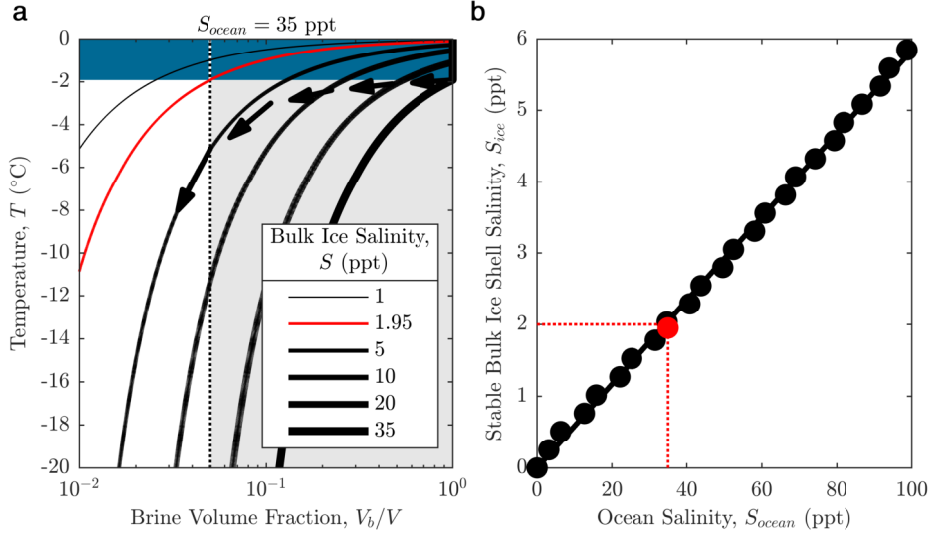


**Figure 10.** Relationship between brine volume fraction, bulk ice salinity, and ocean salinity for terrestrial seawater. (a) Brine volume fraction for sea ice assuming a range of bulk ice salinities, adapted from Butler (2016). (b) Stable bulk ice shell salinity for a range of possible ocean salinities. Data points correspond to the bulk ice salinity where the brine volume fraction equals the percolation threshold ( $\phi_c = 0.05$ ) at a freezing temperature governed by ocean salinity. The red dot represents the specific case shown in a. The line represents a best fit model of the form  $S_{ice} = k_{eq} \times S_{ocean}$ , where  $k_{eq} = 0.0584$ .

Using FREZCHEM, we can extend our analysis to more dilute and more saline terrestrial seawater. We use our brine salinity curve, shown in Fig. 3a, to obtain a freezing temperature for a specified seawater salinity. For seawater salinities up to 100 ppt (note that we limit the upper bound seawater salinity to 100 ppt to ensure our brine volume fraction model is valid, see Section 2.2), we can calculate the bulk ice salinity which produces a brine volume fraction of 0.05 at the freezing temperature. These bulk ice salinities are represented by the black dots in Fig. 10b. We can estimate an effective equilibrium solute distribution coefficient by fitting a linear model of the form  $S_{ice} = k_{eq} \times S_{ocean}$ . These data produce an estimate for an effective equilibrium solute distribution coefficient of 0.0584, represented by the slope of the line shown in Fig. 10b. We note this is lower than the value of 0.067 derived by Wolfenbarger et al. (in press), which might suggest a higher critical porosity should be assumed or that temperature where the per-

colation threshold is applicable should be slightly lower than the freezing temperature even in the case of a very low temperature gradient.

If we further extend this approach to our analog endmember compositions, Fig. 11a shows that the effective equilibrium solute distribution coefficient is not highly sensitive to composition for ocean salinities less than 100 ppt (the ocean salinity range where our model is valid, see Fig. S1, S2 and Table S5). From a best fit model of the form  $S_{ice} = k_{eq} \times S_{ocean}$ , we obtain an effective equilibrium distribution coefficient of  $k_{eq} = 0.059 \pm 0.001$  for a percolation threshold of  $\phi_c = 0.05$  and ocean salinities less than 100 ppt. For the binary endmember cases, our model is valid for salinities up to the eutectic salinity and as such we can explore the full parameter space. Fig. 11b demonstrates that the behavior shown in Fig. 11a does not appear to change significantly when extended to eutectic ocean salinities. At higher salinities, the relationship between stable bulk ice shell salinity and ocean salinity appears to deviate slightly from linear. Nonetheless, we obtain an estimate for effective equilibrium distribution coefficient of  $k_{eq} = 0.062 \pm 0.001$  which is similar to our analog endmember compositions, but still lower than the value of 0.067 derived by Wolfenbarger et al. (in press). Figure 11c demonstrates that the equilibrium solute distribution coefficient increases as the value of the assumed percolation threshold increases. This is consistent with the work of Buffo et al. (2020), where a lower percolation threshold was shown to result in less salt entrainment. Additionally, Fig. 11c suggests that the freezing of a  $SO_4$ -dominated ocean may produce slightly more saline ice than a Cl-dominated ocean ( $k_{eq} = 0.123$  vs.  $k_{eq} = 0.116$  for a percolation threshold of  $\phi_c = 0.1$ ).

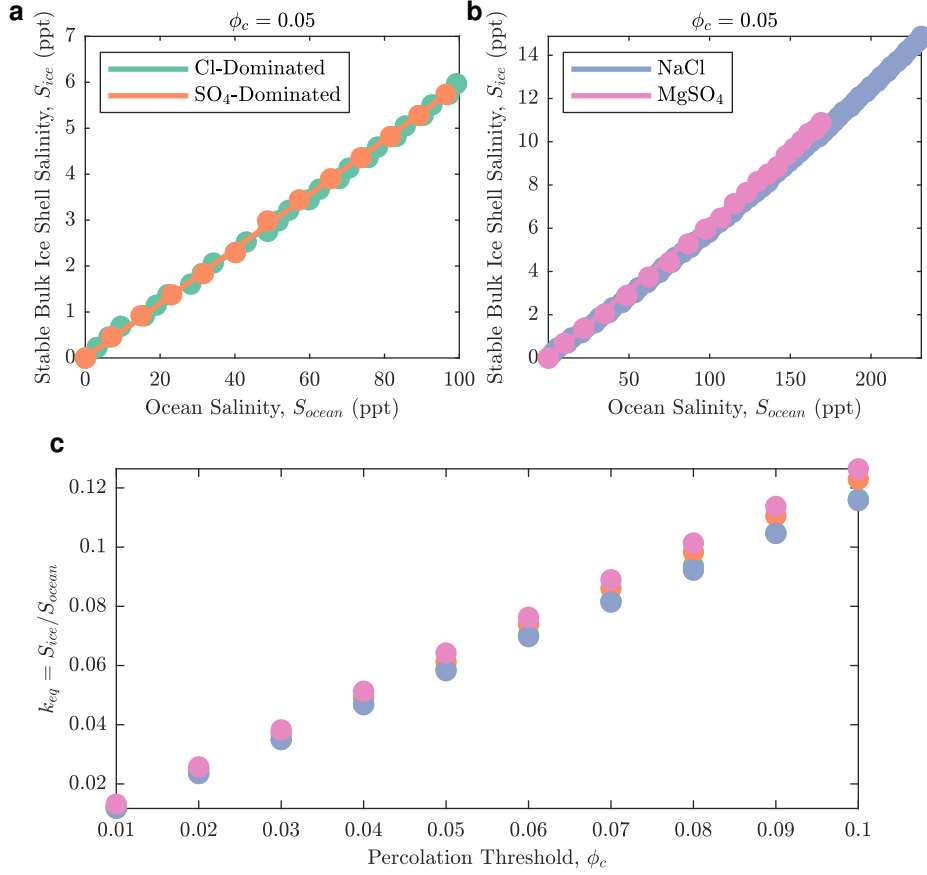


**Figure 11.** Relationship between bulk ice salinity, ocean salinity, and percolation threshold for a range of compositions. Estimates for bulk ice salinity as a function of ocean salinity for our (a) analog endmember compositions and (b) binary endmember compositions, based on a percolation threshold of  $\phi_c = 0.05$ . Data points correspond to the bulk ice salinity where the brine volume fraction equals 0.05 at a freezing temperature governed by the ocean salinity and composition. The lines represent a best fit model of the form  $S_{ice} = k_{eq} \times S_{ocean}$ , where  $k_{eq} = 0.059 \pm 0.001$  for the analog endmember compositions and  $k_{eq} = 0.062 \pm 0.001$  for the binary endmember compositions. (c) Effective equilibrium solute distribution coefficient for a range of percolation thresholds and different ocean compositions.

The magnitude of the percolation threshold in columnar sea ice has been demonstrated to be influenced by the interface morphology of the ice (i.e., the spacing between columnar crystals that make up the cellular microstructural interface) (Maus et al., 2021). Although we do not explore the influence of plate spacing on the critical porosity in this work, previous studies suggest that the critical porosity should decrease as the plate spacing increases (Petrich et al., 2006; Maus et al., 2021). The plate spacing in congelation

ice is inversely proportional to the growth velocity, such that a slower growth (i.e., lower temperature gradient) results in larger plate spacing (Maus, 2020; Maus et al., 2021). For the low growth velocities expected at Europa’s ice-ocean interface (Wolfenbarger et al., in press), this could translate to a lower critical porosity and thus lower bulk ice shell salinity. As the growth velocity approaches zero, the plate spacing approaches infinity and transitions from a cellular to planar microstructural interface morphology. This transition enhances the efficiency of salt rejection and resulting in an even lower bulk ice shell salinity (Wolfenbarger et al., in press). These results suggest that constraining the existence and magnitude of a percolation threshold in columnar ice (i.e., critical porosity) represents a critical step in both predicting the bulk salinity of the ice shell and leveraging the bulk salinity of the ice shell to constrain the salinity of the underlying ocean.

## 4 Conclusions

We have developed a framework for modeling the brine volume fraction of impure water ice as a function of bulk ice salinity and temperature. In this framework we translate the output of a single freezing simulation for a specified ocean composition (performed using the open source aqueous geochemistry software FREZCHEM) to simple polynomial functions of temperature. We validated our framework through comparison with an existing model for sea ice brine volume fraction (Petrich & Eicken, 2017), finding good agreement over the range relevant to Earth applications. Our model represents an improvement to the existing model by (i) extending the temperature range where sea ice brine volume fraction can be estimated down to the eutectic temperature and (ii) following the Gitterman freezing pathway, thought to be more representative of natural sea ice (Marion et al., 1999). Although we apply our framework specifically to Europa, a simple polynomial model for the brine volume fraction of impure water ice can be derived for any system that can be modeled using aqueous geochemistry software, such as FREZCHEM.

Within our framework, we generated models for the brine distribution in Europa’s ice shell, specifically focusing on the fraction which is thermally conductive (either a conductive lid overlying a convective layer or a fully conductive ice shell). We assumed a linear temperature profile that maximized the vertical brine extent and as such our estimates for vertical brine extent represent upper bounds for what is expected at Europa. We modeled the brine volume fraction for four cases of ice shell compositions, consistent with materials observed at Europa’s surface: NaCl, MgSO<sub>4</sub>, a hypothetical Cl-dominated

ocean (analogous to terrestrial seawater), and a hypothetical  $\text{SO}_4$ -dominated ocean (analogous to the European ocean modeled by Zolotov and Shock (2001)), and considered bulk ice salinities ranging from zero to the eutectic salinity.

We found the vertical distribution of brine in an ice shell where impurities are composed of binary species (e.g.,  $\text{Na}^+$  and  $\text{Cl}^-$  or  $\text{Mg}^{2+}$  and  $\text{SO}_4^{2-}$ ) is both lower (i.e., higher eutectic temperature) and far more sensitive to composition (i.e., larger differences in eutectic temperature) than an ice shell where impurities are composed of multiple species (e.g.,  $\text{Na}^+$ ,  $\text{Cl}^-$ ,  $\text{Mg}^{2+}$  and  $\text{SO}_4^{2-}$ ). Although the vertical extent of brine was equivalent for the two analog endmember compositions (because they shared a eutectic temperature), the brine volume fraction for the Cl-dominated ice shell was higher than for the  $\text{SO}_4$ -dominated ice shell across the entire temperature range where brine was thermodynamically stable. Pressure (ice thickness) was found to minimally effect the shape of the phase behavior functions, and thus brine distribution profile; however a larger ice thickness was found to counter-intuitively reduce the fraction of the ice layer where brine is stable although the effect was minor ( $\sim 1\%$ ) across a range of possible thickness.

Assuming the existence of a percolation threshold at a brine volume fraction of 0.05 (consistent with the broadly accepted value for terrestrial congelation sea ice), constraints on the stable bulk ice shell salinity (i.e., the salinity of the ice shell once desalination has stopped) as a function of ocean salinity and composition were obtained. We defined the stable bulk ice shell salinity to be the bulk ice salinity that resulted in a brine volume fraction equal to the percolation threshold at the ocean freezing temperature. The stable bulk ice shell salinity was found to be approximately 6% of the ocean salinity for the assumed percolation threshold. The relationship between percolation threshold and the effective equilibrium solute distribution coefficient was found to be approximately linear, positively correlated, and minimally influenced by composition for critical porosities considered here ( $\phi_c$  ranging from 0.01 to 0.1).

Modeling where brine is thermodynamically stable in Europa's ice shell provides important context for future interpretation of data collected by the upcoming missions to explore Europa and other icy worlds (Howell & Pappalardo, 2020; Grasset et al., 2013). Ice-penetrating radar in particular can identify where liquid water is stable in the ice shell. With improved constraints on ice shell surface composition and temperature, reflections from ice-penetrating radar associated with a eutectic boundary may provide constraints

on bulk ice shell properties, such as the thermal profile (Kalousová et al., 2017) and/or salinity, particularly because the apparent reflectivity is governed by the brine volume fraction (Culha et al., 2020). Constraints on properties of the ice shell will be necessary to robustly constrain the properties of the sub-ice ocean, which represents an important goal in assessing Europa’s habitability. Beyond Europa, missions to other potential ocean worlds such as Enceladus, Titan, Ganymede, and Triton could benefit from this approach, particularly at the science requirements development stage. Future work incorporating the presence of low eutectic surface species (e.g., sulfuric acid, perchlorates) in the framework presented here represents an avenue for understanding how liquid water in the ice shell might serve as a signature of surface-ice-ocean exchange and ultimately Europa’s potential habitability.

## Open Research

The code base used to model the volume fraction of brine and salt in ice for this work is preserved at <https://github.com/nwolfenb/BrineVolumeFraction> and licensed under the GNU General Public License v3.0. Pending acceptance of the manuscript, the code base will be linked to Zenodo.

## Acknowledgments

NSW was supported by the G. Unger Vetlesen Foundation. MGF was supported by the Research England Expanding Excellence in England (E3) fund (grant code 124.18). KMS was supported by the NASA Network for Life Detection project Oceans Across Space and Time (Grant Number: 80NSSC18K1301). DDB was supported by the G. Unger Vetlesen Foundation.

## References

- Assur, A. (1960). *Composition of sea ice and its tensile strength* (Vol. 44). US Army Snow, Ice and Permafrost Research Establishment.
- Barr, A. C., & McKinnon, W. B. (2007). Convection in ice shells and mantles with self-consistent grain size. *Journal of Geophysical Research: Planets*, 112(E2).
- Blankenship, D., Ray, T., Plaut, J., Moussessian, A., Patterson, W., Romero-Wolf, A., ... others (2018). Reason for Europa. *42nd COSPAR Scientific Assembly*, 42, B5-3.

- Blankenship, D. D., Young, D. A., Moore, W. B., & Moore, J. C. (2009). Radar sounding of europa’s subsurface properties and processes: The view from earth. *Europa*, 631–654.
- Brown, M., & Hand, K. (2013). Salts and radiation products on the surface of europa. *The Astronomical Journal*, 145(4), 110.
- Bruzzzone, L., Plaut, J. J., Alberti, G., Blankenship, D. D., Bovolo, F., Campbell, B. A., ... others (2013). Rime: Radar for icy moon exploration. In *2013 IEEE International Geoscience and Remote Sensing Symposium-IGARSS* (pp. 3907–3910).
- Buffo, J., Meyer, C., & Parkinson, J. (2021). Dynamics of a solidifying icy satellite shell. *Journal of Geophysical Research: Planets*, e2020JE006741.
- Buffo, J., Schmidt, B., & Huber, C. (2018). Multiphase reactive transport and platelet ice accretion in the sea ice of mcmurdo sound, antarctica. *Journal of Geophysical Research: Oceans*, 123(1), 324–345.
- Buffo, J., Schmidt, B. E., Huber, C., & Walker, C. C. (2020). Entrainment and dynamics of ocean-derived impurities within europa’s ice shell. *Journal of Geophysical Research: Planets*, 125(10), e2020JE006394.
- Butler, B. M. (2016). *Mineral dynamics in sea ice brines* (PhD Thesis). Prifysgol Bangor University.
- Butler, B. M., & Kennedy, H. (2015). An investigation of mineral dynamics in frozen seawater brines by direct measurement with synchrotron x-ray powder diffraction. *Journal of Geophysical Research: Oceans*, 120(8), 5686–5697.
- Butler, B. M., Papadimitriou, S., Santoro, A., & Kennedy, H. (2016). Mirabilite solubility in equilibrium sea ice brines. *Geochimica et Cosmochimica Acta*, 182, 40–54.
- Carlson, R., Calvin, W., Dalton, J., Hansen, G., Hudson, R., Johnson, R., ... Moore, M. (2009). Europa’s surface composition. *Europa*, 283.
- Chivers, C., Buffo, J., & Schmidt, B. (2021). Thermal and chemical evolution of small, shallow water bodies in europa’s ice shell. *Journal of Geophysical Research: Planets*, 126(5), e2020JE006692.
- Cox, G. F., & Weeks, W. F. (1983). Equations for determining the gas and brine volumes in sea-ice samples. *Journal of Glaciology*, 29(102), 306–316.
- Culha, C., Schroeder, D. M., Jordan, T. M., & Haynes, M. S. (2020). Assessing

- the detectability of europa’s eutectic zone using radar sounding. *Icarus*, 339, 113578.
- Des Marais, D. J., Nuth III, J. A., Allamandola, L. J., Boss, A. P., Farmer, J. D., Hoehler, T. M., ... others (2008). The nasa astrobiology roadmap. *Astrobiology*, 8(4), 715–730.
- Feistel, R. (2008). A gibbs function for seawater thermodynamics for- 6 to 80 c and salinity up to 120 g kg<sup>-1</sup>. *Deep Sea Research Part I: Oceanographic Research Papers*, 55(12), 1639–1671.
- Feistel, R., & Wagner, W. (2006). A new equation of state for h<sub>2</sub>o ice ih. *Journal of Physical and Chemical Reference Data*, 35(2), 1021–1047.
- Geilfus, N.-X., Galley, R., Cooper, M., Halden, N., Hare, A., Wang, F., ... Rysgaard, S. (2013). Gypsum crystals observed in experimental and natural sea ice. *Geophysical research letters*, 40(24), 6362–6367.
- Gitterman, K. (1937). Thermal analysis of seawater. *CRREL TL*, 287.
- Golden, K., Ackley, S., & Lytle, V. (1998). The percolation phase transition in sea ice. *Science*, 282(5397), 2238–2241.
- Golden, K., Eicken, H., Heaton, A., Miner, J., Pringle, D., & Zhu, J. (2007). Thermal evolution of permeability and microstructure in sea ice. *Geophysical research letters*, 34(16).
- Grasset, O., Dougherty, M., Coustenis, A., Bunce, E., Erd, C., Titov, D., ... others (2013). Jupiter icy moons explorer (juice): An esa mission to orbit ganymede and to characterise the jupiter system. *Planetary and Space Science*, 78, 1–21.
- Hand, K., Sotin, C., Hayes, A., & Coustenis, A. (2020). On the habitability and future exploration of ocean worlds. *Space Science Reviews*, 216(5), 1–24.
- Hendrix, A. R., Cassidy, T. A., Johnson, R. E., Paranicas, C., & Carlson, R. W. (2011). Europa’s disk-resolved ultraviolet spectra: Relationships with plasma flux and surface terrains. *Icarus*, 212(2), 736–743.
- Howell, S. M. (2021). The likely thickness of europa’s icy shell. *The Planetary Science Journal*, 2(4), 129.
- Howell, S. M., & Pappalardo, R. T. (2020). Nasa’s europa clipper—a mission to a potentially habitable ocean world. *Nature communications*, 11(1), 1–4.
- Hussmann, H., & Spohn, T. (2004). Thermal-orbital evolution of io and europa. *Icarus*, 171(2), 391–410.

- 874 Kalousová, K., Schroeder, D. M., & Soderlund, K. M. (2017). Radar attenuation  
875 in europa's ice shell: Obstacles and opportunities for constraining the shell  
876 thickness and its thermal structure. *Journal of Geophysical Research: Planets*,  
877 *122*(3), 524–545.
- 878 Kargel, J. S., Kaye, J. Z., Head III, J. W., Marion, G. M., Sassen, R., Crowley,  
879 J. K., ... Hogenboom, D. L. (2000). Europa's crust and ocean: origin, compo-  
880 sition, and the prospects for life. *Icarus*, *148*(1), 226–265.
- 881 Leppäranta, M., & Manninen, T. (1988). The brine and gas content of sea ice with  
882 attention to low salinities and high temperatures.
- 883 Ligier, N., Poulet, F., Carter, J., Brunetto, R., & Gourgeot, F. (2016). Vlt/sinfoni  
884 observations of europa: new insights into the surface composition. *The Astro-*  
885 *nomical Journal*, *151*(6), 163.
- 886 Marion, G., Farren, R., & Komrowski, A. (1999). Alternative pathways for seawater  
887 freezing. *Cold Regions Science and Technology*, *29*(3), 259–266.
- 888 Marion, G., Fritsen, C. H., Eicken, H., & Payne, M. C. (2003). The search for  
889 life on europa: limiting environmental factors, potential habitats, and earth  
890 analogues. *Astrobiology*, *3*(4), 785–811.
- 891 Marion, G., Kargel, J., Catling, D., & Lunine, J. (2012). Modeling ammonia-  
892 ammonium aqueous chemistries in the solar system's icy bodies. *Icarus*,  
893 *220*(2), 932–946.
- 894 Marion, G., & Kargel, J. S. (2007). *Cold aqueous planetary geochemistry with*  
895 *frezchem: From modeling to the search for life at the limits*. Springer Science &  
896 Business Media.
- 897 Marion, G., Kargel, J. S., Catling, D. C., & Jakubowski, S. D. (2005). Effects of  
898 pressure on aqueous chemical equilibria at subzero temperatures with applica-  
899 tions to europa. *Geochimica et Cosmochimica Acta*, *69*(2), 259–274.
- 900 Marion, G., Millero, F., & Feistel, R. (2009). Precipitation of solid phase calcium  
901 carbonates and their effect on application of seawater s a-t-p models. *Ocean*  
902 *Science*, *5*(3), 285–291.
- 903 Maus, S. (2020). The plate spacing of sea ice. *Annals of Glaciology*, *61*(83), 408–  
904 425.
- 905 Maus, S., Schneebeli, M., & Wiegmann, A. (2021). An x-ray micro-tomographic  
906 study of the pore space, permeability and percolation threshold of young sea

- ice. *The Cryosphere*, 15(8), 4047–4072.
- McCord, T. B., Hansen, G. B., Fanale, F., Carlson, R., Matson, D., Johnson, T., . . .  
others (1998). Salts on europa’s surface detected by galileo’s near infrared  
mapping spectrometer. *Science*, 280(5367), 1242–1245.
- McKinnon, W. B. (1999). Convective instability in europa’s floating ice shell. *Geo-  
physical Research Letters*, 26(7), 951–954.
- Millero, F. J., Feistel, R., Wright, D. G., & McDougall, T. J. (2008). The com-  
position of standard seawater and the definition of the reference-composition  
salinity scale. *Deep Sea Research Part I: Oceanographic Research Papers*,  
55(1), 50–72.
- Mitri, G., & Showman, A. P. (2005). Convective–conductive transitions and sensi-  
tivity of a convecting ice shell to perturbations in heat flux and tidal-heating  
rate: Implications for europa. *Icarus*, 177(2), 447–460.
- Nelson, K. H., & Thompson, T. G. (1954). Deposition of salts from sea water by  
frigid concentration.
- Ojakangas, G. W., & Stevenson, D. J. (1989). Thermal state of an ice shell on eu-  
ropa. *Icarus*, 81(2), 220–241.
- Petrich, C., & Eicken, H. (2017). Overview of sea ice growth and properties. *Sea ice*,  
1–41.
- Petrich, C., Langhorne, P., & Eicken, H. (2011). Modelled bulk salinity of growing  
first-year sea ice and implications for ice properties in spring. In *Proceedings  
of the international conference on port and ocean engineering under arctic  
conditions*.
- Petrich, C., Langhorne, P. J., & Sun, Z. F. (2006). Modelling the interrelationships  
between permeability, effective porosity and total porosity in sea ice. *Cold Re-  
gions Science and Technology*, 44(2), 131–144.
- Pringle, D., Miner, J., Eicken, H., & Golden, K. (2009). Pore space percolation in  
sea ice single crystals. *Journal of Geophysical Research: Oceans*, 114(C12).
- Ringer, W. (1906). De varanderingon in samenstelling van zeewater bij het  
bevriezen. *Chemisch Weekblad*, 3(15), 223–249.
- Ruiz, J., Montoya, L., López, V., & Amils, R. (2007). Thermal diapirism and the  
habitability of the icy shell of europa. *Origins of Life and Evolution of Bio-  
spheres*, 37(3), 287–295.

- Shematovich, V. (2018). Ocean worlds in the outer regions of the solar system. *Solar System Research*, 52(5), 371–381.
- Soderlund, K. M., Kalousová, K., Buffo, J. J., Glein, C. R., Goodman, J. C., Mitri, G., ... others (2020). Ice-ocean exchange processes in the jovian and saturnian satellites. *Space Science Reviews*, 216(5), 1–57.
- Squyres, S. W., Reynolds, R. T., Cassen, P. M., & Peale, S. J. (1983). Liquid water and active resurfacing on europa. *Nature*, 301(5897), 225–226.
- Steinbrügge, G., Voigt, J. R., Wolfenbarger, N. S., Hamilton, C., Soderlund, K., Young, D., ... Schroeder, D. M. (2020). Brine migration and impact-induced cryovolcanism on europa. *Geophysical Research Letters*, 47(21), e2020GL090797.
- Tobie, G., Choblet, G., & Sotin, C. (2003). Tidally heated convection: Constraints on europa's ice shell thickness. *Journal of Geophysical Research: Planets*, 108(E11).
- Trumbo, S. K., Brown, M. E., & Hand, K. (2019). Sodium chloride on the surface of europa. *Science advances*, 5(6), eaaw7123.
- Turner, A. K., Hunke, E. C., & Bitz, C. M. (2013). Two modes of sea-ice gravity drainage: A parameterization for large-scale modeling. *Journal of Geophysical Research: Oceans*, 118(5), 2279–2294.
- Vancoppenolle, M., Madec, G., Thomas, M., & McDougall, T. J. (2019). Thermodynamics of sea ice phase composition revisited. *Journal of Geophysical Research: Oceans*, 124(1), 615–634.
- Vilella, K., Choblet, G., Tsao, W.-E., & Deschamps, F. (2020). Tidally heated convection and the occurrence of melting in icy satellites: Application to europa. *Journal of Geophysical Research: Planets*, 125(3), e2019JE006248.
- Wolfenbarger, N., Buffo, J., Soderlund, K., & Blankenship, D. (in press). Ice shell structure and composition of ocean worlds: Insights from accreted ice on earth. *Astrobiology*.
- Zolotov, M. Y., & Shock, E. L. (2001). Composition and stability of salts on the surface of europa and their oceanic origin. *Journal of Geophysical Research: Planets*, 106(E12), 32815–32827.
- Zubov, N. N. (1945). *L'dy arktiki*. Izdatel'stvo glavsevmorputi.